

Article

Release, Migration, Sorption, and (Re)Precipitation of U during Peraluminous Granite Alteration under Oxidizing Conditions in Central Portugal

Marina M. S. Cabral Pinto ^{1,2,*} , Maria M. V. G. Silva ¹, Ana M. R. Neiva ¹,
Fernanda Guimarães ³ and Paulo B. Silva ³

¹ Department of Earth Sciences, University of Coimbra, Portugal, 3000-272 Coimbra, Portugal; mmvsilva@ci.uc.pt (M.M.V.G.S.); neiva@ci.uc.pt (A.M.R.N.)

² Geosciences Department, GeoBioTec Research Center, University of Aveiro, Portugal, 3810 Aveiro, Portugal

³ LNEG—National Laboratory of Energy and Geology, Rua da Amieira, Apartado 1089, 4466-956 São Mamede de Infesta, Portugal; Fernanda.Guimaraes@lneg.pt (F.G.); paulobravosilva@gmail.com (P.B.S.)

* Correspondence: mcp@uc.pt; Tel.: +351-96-433-2189

Received: 25 November 2017; Accepted: 9 March 2018; Published: 12 March 2018

Abstract: In this work, in order to study the release, migration, sorption, and (re)precipitation of uranium (U) during alteration under oxidizing conditions, we carried out a systematic study using scanning electron microscopy, X-ray maps, and electron microprobe analyses on uranium minerals—such as uraninite, coffinite, saleeite, meta-saleeite, and thorite—and U-bearing minerals—such as xenotime, monazite, apatite, and zircon—from unaltered and altered Variscan peraluminous granites and related hydrothermal brecciated uranium–quartz veins. The paragenetic sequence of the granite and the mineralized quartz veins from Vale the Abrutiga is presented. Uraninite is magmatic in origin and occurs mainly in unaltered granite; it is rare in altered granite, and was not found in the mineralized quartz veins. Uraninite from the altered granite was fractured and hydrated; it had radioactive damage halos filled with late pyrite, U–S-bearing phases, and Fe oxyhydroxides; its analytical totals were also lower than in the uraninite from the unaltered granite. The alteration zones and crystal rims were poorer in U (86.7 wt. % UO₂) than in the cores and unaltered zones (90.2 wt. % UO₂), and some uraninite crystals were replaced by coffinite, which resulted from uraninite alteration. The U contents in the coffinite crystals ranged between 65.0 wt. % UO₂ in the rims to 84.0 wt. % UO₂ in the cores of the crystals. Thorite was found in all of the granite samples, and its composition was variable from 0.5 wt. % UO₂ to 10.4 wt. % UO₂. Some thorite seemed to be primary, whereas the other thorite was related to the granite alteration, replaced apatite and monazite, was associated with xenotime, and filled the fractures of several minerals. In the altered granite, thorite had low UO₂ contents (0.46 wt. %) in the fractured crystal zones. Monazite from the altered granite had a pervasive porosity; some crystals were formed by the alteration of apatite, and were frequently replaced by thorite. Monazite and xenotime from the altered granite and hydrothermal veins had lower U contents than these minerals from the unaltered granite. In the altered granite, xenotime crystals were zoned, and their cores were richer in U than the rims. Apatite from the altered granite was fractured, showed dissolution, and had lower U and P contents than the apatite from the unaltered granite. In the quartz veins, apatite crystals were replaced by uranium phosphates and had high U contents (~1.1 wt. % UO₂). In the quartz veins, zircon rims had an extraordinary U enrichment (up to 18 wt. % UO₂). The most altered rims of chlorite and anatase from the quartz veins were partially replaced by U-bearing Fe oxyhydroxides containing up to 5.7 wt. % UO₂. Meteoric water warmed by deep circulation through granite faults, shear zones, and quartz veins became enriched in U, P, and Mg due to the solubilization of mainly uraninite, coffinite, thorite, monazite, apatite, and chlorite. Uranium from these solutions was later adsorbed on Fe oxyhydroxides and the weathered surfaces of anatase, zircon, and apatite, or precipitated as saleeite and meta-saleeite on the surface of Fe minerals and the apatite-weathered surface due to local saturation.

Keywords: uranium minerals; uranium migration; secondary uranium phosphate mineralization; central Portugal

1. Introduction

Uranium is a structural constituent in nearly 200 mineral species [1], and more than 200 valid uranium-bearing mineral phases were described by [2]. These minerals are interesting as an energy resource, and play a role in environmental problems associated with the disposal of radioactive waste materials, mining contamination, and the remediation of contaminated sites. Therefore, uranium minerals have received an increasing amount of attention [3].

Uraninite is the most important uranium mineral in terms of abundance and economic value [4], as well as the principal ore mineral in Portuguese uranium mineral deposits [5]. In general, it occurs in granites, pegmatites, and associated quartz veins. Uraninite is unstable in acid and oxidizing conditions such as those found in acid hydrothermal and meteoric fluids; it is easily dissolved, and is probably the most important source of dissolved U in groundwater emanating from weathered granite terrains [6–12]. Other minerals from magmatic rocks (e.g., thorite, huttonite, thorianite, monazite, titanite, xenotime, allanite, zircon) host uranium, and their alteration by acid hydrothermal or meteoric fluids is also a source of dissolved U in hydrothermal fluids or surface waters and groundwater; many uranium deposits are derived from them [10,13–16].

The principal mechanism of the dissolution of U from minerals is oxidation, with Fe^{III} as the oxidant [17]. Fe^{III} is produced by the oxidation of pyrite, which is usually associated with the uranium minerals. The uranyl ion (UO₂²⁺) and its complexes are soluble in water, and can be transported over kilometers. Changes in aqueous chemistry (pH, Eh, ionic potential), temperature, and pressure lead to the precipitation of new uranium minerals such as uranyl oxyhydroxides, carbonates, silicates, phosphates, vanadates, molybdates, arsenates, etc. [4,14,15,18,19]. Uranyl ion can also be sorbed onto Fe oxyhydroxides [20–23]. Under reducing conditions, U⁴⁺ precipitates as an insoluble UO₂ phase.

Uranium mineralizations are widespread in central Portugal, and some of them were exploited, with interruptions, until the 1980s. Currently, the production is stopped. Although these uranium mines are small, Portugal is the third or fourth country with major resources in Western Europe [24]. Portuguese uranium deposits are mostly uranium–quartz veins related to uranium-bearing Variscan granites, which cut the granites and their contact metamorphic aureole. The structural control of the mineralization is of extreme importance, and locally, the epithermal uranium mineralization overlays a sulfide mesothermal mineralization or a cassiterite–wolframite hypothermal mineralization [5,15,25,26].

There are various generations of uraninite in Portuguese uranium deposits. Coffinite is a reduced U-mineral that is contemporaneous with the last generation of uraninite [5]. Portuguese uranium deposits also contain U⁶⁺ mineral species such as oxides, phosphates, silicates, sulfates, and arsenates [5,15,25,27].

The abandoned Vale de Abrutiga uranium mine is located in central Portugal close to Variscan peraluminous biotite granite, and is a uranium phosphate mine that was exploited until 1989. The granite has a mean of 10 ppm U, presents hydrothermal alteration, and is the most probable source of U [15]. The granite contains uraninite and thorite, while coffinite is also present in the hydrothermally altered granite. These minerals do not occur in the mineralized quartz veins. The ore mineral is saleeite, meta-saleeite, and other U-phosphate phases with similar compositions to saleeite but different H₂O concentrations, which occur as aggregates of lamellar crystals in millimeter-sized veins.

This study aims to understand the release of U from minerals in the unaltered granite, its migration within the hydrothermal fluids in the altered granite during oxidation conditions, its sorption and (re)precipitation in the mineralized quartz veins under oxidizing conditions, and to point out the genesis of the secondary U mineralization. Therefore, a systematic study using scanning electron microscopy, and obtaining X-ray maps and electron microprobe analyses of the uranium minerals (uraninite, coffinite, thorite, saleeite, and meta-saleeite) and uranium-bearing minerals (xenotime,

monazite, apatite, zircon, chlorite, and anatase) is presented. The samples are from three different locals: (a) the unaltered biotite granite, (b) the hydrothermally altered biotite granite, and (c) from related hydrothermally uranium quartz veins.

2. Geological Setting

The coarse–very coarse-grained porphyritic biotite Variscan granite (308 ± 11 Ma, [28]) is located in central Portugal and forms the border of the Beiras batholith. The granitic magma intruded the Neoproterozoic to Cambrian Beiras Group (Figure 1). This consists of chlorite phyllite with intercalations of metagraywacke, metasandstone, and metaconglomerates, and minor thin marble and dolomitic marble beds. The intrusion produced an outer zone of contact metamorphism consisting of mica schist, and an inner zone of discontinuous hornfels contact metamorphic aureole. Close to the contact, the granite shows a plane-linear fabric due to the N–S to 10° E orientation of feldspar phenocrysts caused by magmatic flux. NE–SW—and also some NW–SE—aplite, aplite–pegmatite, and pegmatite veins, as well as numerous quartz veins, cut the granite.

The biotite granite is peraluminous, and contains feldspar phenocrysts that are $2\text{ cm} \times 5\text{ cm}$ on average, with some reaching $10\text{ cm} \times 15\text{ cm}$. Euhedral, a $1\text{ cm} \times 1.5\text{ cm}$ greenish blue cordierite, is abundant close to the contact with the country rock. The granite also contains microgranular enclaves and xenoliths. The granite is hydrothermally altered where affected by faults and shear zones, and the altered zone is locally very deep (up to 50 m).

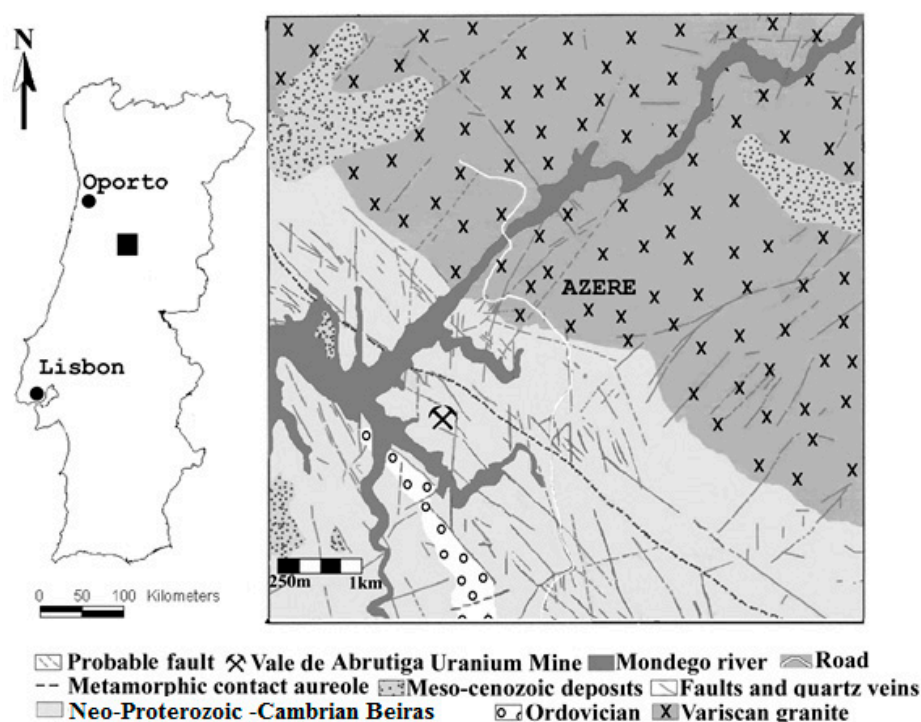


Figure 1. Location and geological map of the Variscan Beiras granite and related mineralized hydrothermal quartz veins.

The uranium quartz veins that cut the country rock phyllites are thin (from the order of millimeters), brecciated, and aligned along the $N 45^\circ W$ direction, which is the orientation of the phyllite cleavage and the contact with the granite country rock. They fill old NW–SE faults (Figure 1). The U-mineralization consists of secondary U-phosphates—mainly saleeite and meta-saleeite—and occurs in the intersection of this fault system with late $N 10^\circ$ – 25° W faults. However, it also occurs disseminated in the phyllite at vein walls. The epithermal uranium mineralization of quartz veins overlays a hydrothermal wolframite–sulfide mineralization [15].

The abandoned Vale de Abrutiga uranium mine is located in the phyllites, close to the granite (Figure 1), with a mottled schists-contact aureole with a thickness of up to 1.5 km. It produced a total of 93,325 Kg U_3O_8 , with a grade of 1 kg U_3O_8 /ton, and operated from 1982 until 1989, with an interruption from 1983 to 1984 (National Uranium Enterprise reports). The mineralization was disseminated from the surface to about 50 m, and the mine was an open pit.

3. Analytical Methods

Sampling collection was divided in three “sample types”: (a) unaltered granite, (b) hydrothermally altered granite, and (c) mineralized quartz veins.

The unaltered granite was collected in quarries, but the hydrothermally altered granite was obtained from cuttings-altered areas. Samples from the mineralized quartz veins were collected in drill cores, which were provided by National Uranium Enterprise.

The point counting and modal abundances of the minerals were done on 24 thin sections from hydrothermally altered granite and 24 thin sections from unaltered granite in order to have quantitative information of mineral abundance. Differences between minerals compositions from the altered and unaltered granites were performed (*t*-Student test) using the IBM©SPSS (v. 21) software package.

The mineralogical characteristics were examined using reflected and transmitted light microscopy, secondary electron imaging (SEI), and backscattered electron imaging (BSE) in an electron microprobe. The electron microprobe analysis was performed on polished thin sections using two electron microprobes, a JEOL JX8600 at the Department of Earth Sciences, University of Bristol, United Kingdom (UK), and a JEOL 8500-F, at LNEG, S. Mamede de Infesta, Portugal. The operating conditions for the JEOL JX8600 are given in [15]. The quantitative analysis and X-ray dot maps performed with the JEOL 8500-F were obtained with the five wavelength Spectrometers installed. Operating conditions were 20 kV accelerating voltage and 100 nA current. Beam diameter was kept at 1 μ m. Counting times varied between 20 s for F, Si, Fe, P, Al, and Ca; and 60 s for Ce, La, Hf, Zr, Pb, Dy, Pr, Nd, Y, Ho, Er, Sm, Lu, Gd, Yb, Th and U, in order to improve statistics and count rates. Detection limits obtained for rare earth elements (REE) ranged between 124–252 ppm. The elements, standards, and lines used were: Si ($Fe_3Al_2Si_3O_{12}$, $K\alpha$); Dy (DyP_5O_{14} , $L\alpha$); Fe (Fe_2O_3 , $K\alpha$); F (CaF, $K\alpha$); P ($Ca_5(PO_4)_3F$, $K\alpha$); Hf (Hf, $L\alpha$); Pb (PbS, $L\alpha$); Al (Al_2O_3 , $K\alpha$); Ca ($Ca_5(PO_4)_3F$, $K\alpha$); Pr (PrP_5O_{14} , $L\beta$); Ce (CeP_5O_{14} , $L\alpha$); Ti (TiO_2 , $K\alpha$); Nd (NdP_5O_{14} , $L\alpha$); La (LaP_5O_{14} , $L\alpha$); Y (YAG, $L\alpha$); Ho (HoP_5O_{14} , $L\alpha$); Th (ThO_2 , $M\alpha$); Er (ErP_5O_{14} , $L\alpha$); U (UO_2 , $M\beta$); Sm (SmP_5O_{14} , $L\alpha$); Zr ($ZrSiO_4$, $L\alpha$); Lu (LuP_5O_{14} , $L\alpha$); Gd (GdP_5O_{14} , $L\alpha$); and Yb (YbP_5O_{14} , $L\alpha$). The concentrations of Dy, Hf, Pr, Nd, Ho, Er, Sm, Lu, Gd, and Yb were analyzed using a LiFH crystal, and mounted on a spectrometer that used a smaller diameter Rowland Circle, allowing higher count rates, although poorer wavelength resolution. Tb, Tm, and Eu were not measured with this microprobe. Data reduction was made by the use of the Armstrong method, which equips Jeol microprobes. X-ray lines and background offsets were carefully selected in order to minimize interferences and also apply necessary corrections. Overlapping peaks and backgrounds were identified after individual wavelength spectral scans on standards and specimens. The percentage of overlap was first determined by the calculation routine performed by the machine on the chosen standards. The interference of $ThM\beta$ on $UM\alpha$, and $YM\alpha$ on $PbM\beta$, was eliminated by the use of $ThM\alpha$ $UM\beta$ and $PbL\alpha$, respectively. Also, the interference of $LaL\beta$ in $PrL\alpha$ was eliminated by the use of $PrL\beta$.

4. Petrographic Relations

The paragenetic sequence of the granite and the mineralized quartz veins from Vale the Abrutiga is present in Figure 2.

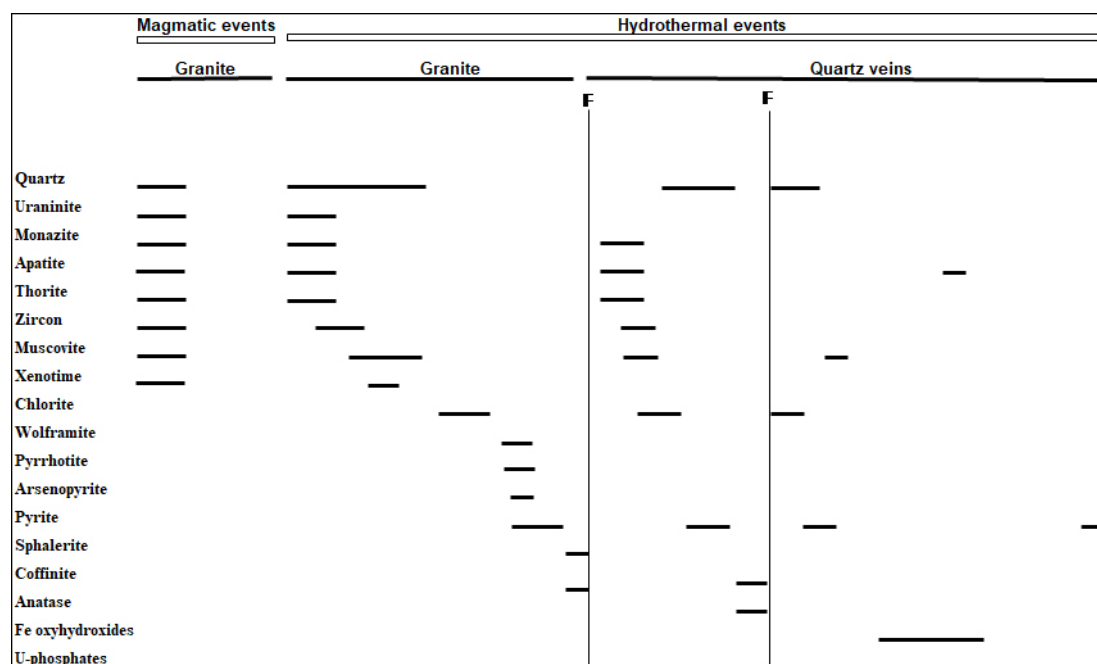


Figure 2. Paragenetic sequence of the accessory minerals and quartz of the granite, and of the mineralized quartz veins from Vale the Abrutiga. F: fault.

4.1. Granite

The unaltered porphyritic, biotite Variscan granite contains quartz, microperthitic microcline, plagioclase, biotite, cordierite, rare primary muscovite, tourmaline, apatite, zircon, monazite, xenotime, uraninite, thorite, fluorite, ilmenite, rutile, pyrite, and rare native gold and silver. It contains phenocrysts of microperthitic microcline and andesine–oligoclase [28,29]. The hydrothermally altered biotite granite contains the same minerals, and also has secondary muscovite, chlorite, titanite, calcite, very rare epidote, allanite, coffinite, thorite, and monazite.

Quartz is anhedral, with slight undulatory extinction, and contains inclusions of feldspars, micas, monazite, xenotime, uraninite, coffinite, thorite, rutile, and pyrite. There are several generations of quartz. The quartz from altered granite is strongly fractured, and is frequently filled by alteration minerals.

Plagioclase has inclusions of biotite, muscovite, zircon, monazite, ilmenite, pyrite, uraninite, and thorite. In the altered granite, both feldspars are vacuolated, fractured, and altered to secondary muscovite, and plagioclase is replaced by calcite.

Biotite contains inclusions of zircon, apatite, monazite, xenotime, ilmenite, pyrite, uraninite, and thorite. Locally, biotite occurs as intergrowth with primary muscovite. In the altered granite, biotite is altered to chlorite. Titanite is related to chloritization. Primary muscovite is subhedral, and is much less abundant than biotite. Muscovite contains quartz, zircon, apatite, monazite, and xenotime inclusions. Cordierite is euhedral, and generally does not contain inclusions in the unaltered granite. In the altered granite, cordierite is altered to a mixture of secondary muscovite and chlorite.

Tourmaline replaces feldspars and micas, is euhedral to anhedral, and is pleochroic from ω —pale yellow to ε —greenish yellow. The euhedral crystals are slightly zoned, with a green rim and a light bluish-green core. Crystal dimensions are 0.5 mm \times 3 mm on average, and locally show zircon inclusions.

Uraninite occurs in the unaltered granite, but it is rare in the altered granite. Uraninite crystals are small (5–10 μm) and occur enclosed in quartz, feldspar, micas, ilmenite, chlorite, and apatite. Uraninite is commonly associated with pyrite, zircon, and monazite, and produced radioactive damage halos. Euhedral crystals are restricted to unaltered granite and nearly homogeneous uraninite predominates

over zoned grains; backscattered electron imaging did not reveal zonation. In the altered granite, uraninite is fractured and vacuolated (Figure 3a–c), and radioactive damage halos are filled with late pyrite, U–S-bearing phases, and Fe oxyhydroxides (Figure 3b,c).

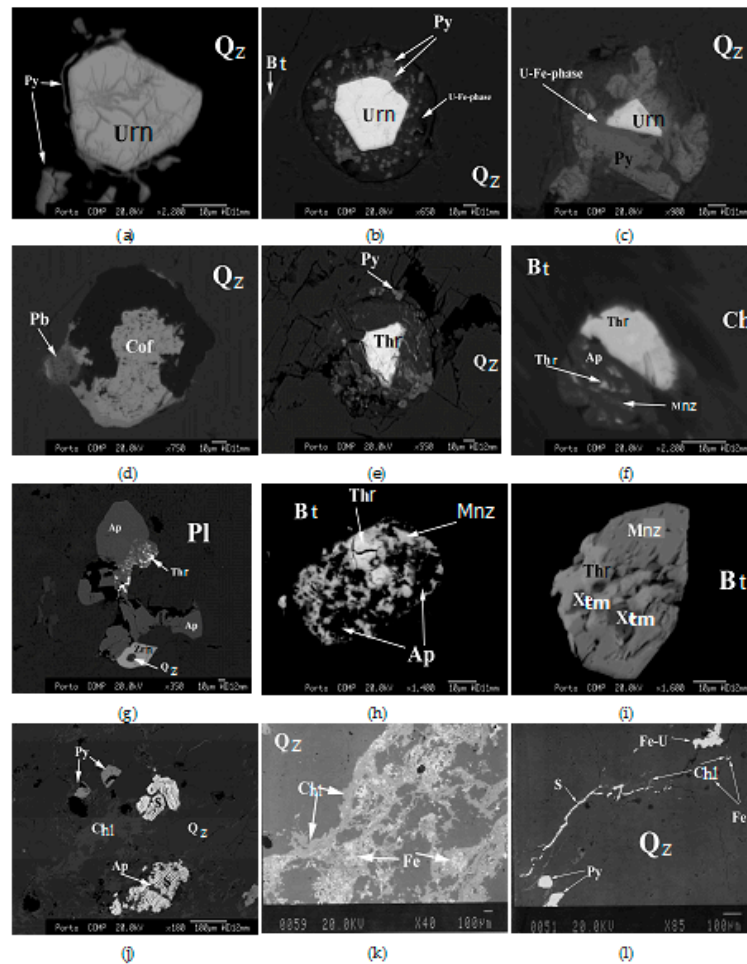


Figure 3. Backscattered images of minerals from the Variscan granite (a–i) and related mineralized hydrothermal quartz veins (j–l), central Portugal. Symbols: Ap: apatite, B: biotite, Cl: chlorite, Cof: coffinite, Fe: Fe oxyhydroxides, Fe-U: U-bearing Fe oxyhydroxides, Mon: monazite, Py: pyrite, Pb: Pb oxide, Q: quartz, S: saleeite, meta-saleeite, and Fe-saleeite, Th: thorite, U: uraninite, U-Fe-phase: U-Fe bearing phases, Xe: xenotime, Z: zircon. (a) Zoned crystal of uraninite (Urn) enclosed in quartz (Qz) grain, with the radioactive damage zone filled with pyrite (Py); (b) Fractured and zoned crystal of uraninite (Urn) enclosed in quartz (Qz); (c) Crystal of uraninite (Urn) enclosed in fractured quartz (Qz), associated with U–S–Fe- phases (U-Fe-phase) and pyrite (Py); (d) Corroded crystal of coffinite (Cof) enclosed in fractured quartz (Qz), associated with Pb oxide; (e) Subhedral crystal of thorite (Thr) with the radioactive damage zone filled with late pyrite (Py). Thorite is enclosed in fractured quartz (Qz) grains; (f) Apatite (Ap) replaced by monazite (Mnz), which is replaced by thorite (Thr), enclosed in biotite (Bt), and enclosed in chloritized (Chl) biotite (Bt); (g) Fractured crystal of apatite (Ap) replaced by thorite (Thr) and associated with zircon (Zrn), enclosed in plagioclase (Pl); (h) Fractured crystal of apatite (Ap), replaced by monazite (Mnz), which is replaced by thorite (Thr), and enclosed in biotite (Bt); (i) Fractured crystal of monazite (Mnz), replaced by thorite (Thr) and xenotime (Xtm), and enclosed in chloritized biotite (Bt); (j) Saleeite (S) replacing apatite (Ap), and filling quartz (Qz) fractures. Chlorite (Chl) enclosed in quartz; (k) Chlorite (Chl) weathered to Fe oxyhydroxides (Fe, filling fractures in the mineralized quartz (Qz) veins); (l) Saleeite (S), filling fractures in the mineralized quartz (Qz) veins, associated with U-rich Fe oxyhydroxides (Fe-U), pyrite (Py), and chlorite (Chl).

Coffinite occurs in altered granite, and is enclosed in quartz. Coffinite crystals are anhedral to subhedral, and have dimensions of $40\ \mu\text{m} \times 50\ \mu\text{m}$. Crystals are corroded and vacuolated; a core–rim within single crystals is clearly visible under backscattered electron (BSE) imaging (Figure 3d) and X-ray element mapping, where the altered rims of the crystals are relatively darker than the unaltered areas. Some coffinite grains replace uraninite crystals.

Thorite was found in all of the granite samples; however, it occurs mainly in the hydrothermally altered granite. Thorite occurs typically as small (5–8 μm) crystals, with most of them anhedral to subhedral. Some grains are strongly zoned, and the within-grain compositional variability is large. It is usually hosted in the major minerals of the granite, including quartz, biotite, muscovite, chlorite, apatite, and plagioclase, which is locally associated with zircon. In altered granite, thorite fills the fractures of other minerals, such as apatite, monazite, and biotite (Figure 3e–i)—mainly in their rims—and seems to replace monazite along fractures (Figure 3f–i), which is associated with xenotime (Figure 3i).

Zircon is zoned in granite, enclosed in biotite and apatite, and has inclusions of quartz. It is light brown to colorless, presents a very weak pleochroism, and is mainly euhedral and subhedral, with variable dimensions, from $10\ \mu\text{m} \times 10\ \mu\text{m}$ to $40\ \mu\text{m} \times 70\ \mu\text{m}$.

Apatite is euhedral and subhedral. Apatite crystals are frequently fractured and have variable dimensions, from $200\ \mu\text{m} \times 300\ \mu\text{m}$ to $20\ \mu\text{m} \times 30\ \mu\text{m}$. It occurs mainly enclosed in biotite and plagioclase, and contains inclusions of zircon and uraninite. In the altered granite, crystals of apatite have a pervasive porosity, indicating the dissolution of apatite with the formation of calcite. It is also highly fractured, and is replaced by monazite and thorite (Figure 3f–h). Where alteration is more extensive, apatite is practically pseudomorphosed by thorite (Figure 3h).

Xenotime occurs as euhedral, zoned, fractured crystals ($\sim 10\ \mu\text{m} \times 12\ \mu\text{m}$), is enclosed in quartz and muscovite, associated with zircon, and locally seems to cut micas and plagioclase. As stated above, it also occurs associated with thorite, where it is anhedral (Figure 3i). Allanite occurs associated with epidote and chloritized biotite in the altered granite. The crystals are anhedral and are mostly $50\ \mu\text{m}$ to $100\ \mu\text{m}$ in size; they are rarely up to $150\ \mu\text{m}$.

Ce-monazite is very light yellow, presents a very weak pleochroism, and is commonly hosted in biotite and plagioclase. In general, it occurs as subhedral crystals ($15\ \mu\text{m} \times 15\ \mu\text{m}$); however, in altered granite, the grains ($15\ \mu\text{m} \times 10\ \mu\text{m}$) are anhedral, corroded, and fractured, and also contain a scattering of holes or tiny inclusions of quartz. Locally, it replaces apatite and is replaced by thorite (Figure 3h), which also occurs along its fractures. The altered monazite, which is close to the thorite, developed a high porosity, and a distinct interface could be observed between the altered and the unaltered zones in the monazite (Figure 3i).

4.2. Mineralized Quartz Veins

The hydrothermal quartz veins are brecciated and composed of quartz, muscovite, chlorite, pyrite, apatite, Fe oxyhydroxides, saleeite, meta-saleeite, and other U-phosphate phases. The accessory minerals are monazite, zircon, xenotime, ferberite, hübnerite, pyrrhotite, arsenopyrite, sphalerite, and Ti oxides.

Quartz is anhedral and fractured, with muscovite, chlorite, pyrite, Fe oxyhydroxides, and U-phosphates filling the fractures (Figure 3j–l). There are several generations of quartz [15,25]. Xenotime is rare, small, and occurs between—or enclosed in—the second and third generations of quartz, or enclosed in the U-phosphates, and is associated with zircon.

Zircon is anhedral to subhedral, with larger dimensions than in the granite (up to $50\ \mu\text{m} \times 120\ \mu\text{m}$), and is generally enclosed in quartz. Zoned, dissolved, and fractured zircon grains were found, and the fractures were filled with quartz and Fe oxyhydroxides. Apatite is rare, subhedral, and is always dissolved and replaced by U-phosphates (Figure 3j). Its dimensions range from $10\ \mu\text{m} \times 10\ \mu\text{m}$ to $100\ \mu\text{m} \times 150\ \mu\text{m}$. Monazite occurs enclosed in quartz, muscovite, Fe oxyhydroxides, and also between

quartz crystals. It is anhedral, bigger than in granite (average dimension is $25 \mu\text{m} \times 40 \mu\text{m}$), frequently dissolved, and some of its vacuoles are filled with quartz.

Muscovite and chlorite also occur in several generations; locally, they are intergrown, surrounded by U-bearing Fe oxyhydroxides, and in contact with saleeite and meta-saleeite. Chlorite is weathered to Fe oxyhydroxides (Figure 3k). Ti oxides (anatase) are dark reddish brown, and the crystals are often dissolved and vacuolated and surrounded by uranium-rich Fe oxyhydroxides.

Fe oxyhydroxides are abundant in the mineralized quartz veins. They are reddish brown and reddish orange, often banded, locally show colloidal textures, fill fractures and microfractures, surround the other crystals, occur as masses, frequently replace muscovite, chlorite, and Ti oxides, and are surrounded by uranium phosphates.

Macroscopic crystals of U-phosphates occur in the mineralized quartz veins and the adjacent phyllite, forming millimeter-sized veins that locally cut pyrite. Saleeite and meta-saleeite were not distinguished by Energy Dispersive X-ray Spectroscopy (EDS) during the Scanning Electron Microscopy (SEM) investigation or examination. They are the last minerals, filling microfractures and the space between grain boundaries (Figure 3l), have a yellowish and brownish color, and occur as aggregates of lamellar crystals, mostly in the range $5 \mu\text{m} \times 20 \mu\text{m}$. They are often associated with pyrite and chlorite; they also surround the Fe-U oxyhydroxides, and replace U-rich apatite.

5. Chemical Composition of U Minerals and U-bearing Minerals

In this section, chemical analyses of uraninite, coffinite, thorite, zircon, xenotime, monazite, apatite, saleeite, and meta-saleeite from unaltered and altered granites and from hydrothermal quartz veins are presented. X-ray element maps of uraninite, coffinite, thorite, xenotime, apatite, and (meta)saleeite are also presented in order to study the release, migration, sorption, and (re)precipitation of U during alteration under oxidizing conditions.

5.1. Uraninite

Chemical analyses of uraninite (UO_2) are given in Table 1 material (Table S1). The average chemical formula of uraninite from the unaltered granite is $\text{U}_{0.93}\text{Pb}_{0.05}\text{Th}_{0.02}\text{Fe}_{0.02}$ (Table 1), ranging between 0.905–0.949 (1 s) a.p.f.u., and with a mean value of 0.927 a.p.f.u. Thorium contents are low, and Pb is the second cation in uraninite (Table 1). The uraninite is poor in Y (mean concentrations of 0.006 a.p.f.u.) and REE (mean concentrations of ≤ 0.002 a.p.f.u. light rare earth elements (LREE) (Ce + Pr + Nd + Sm) and of ≤ 0.001 a.p.f.u. heavy rare earth elements (HREE) 2.3 (Gd + Dy + Ho + Er + Yb + Lu)). Silicon and Al were present with very low contents of 0.007 a.p.f.u. and 0.002 a.p.f.u., respectively, (Table 1), but Si reached 0.023 a.p.f.u., and Al up to 0.012 a.p.f.u. [15]. Calcium and Fe mean contents were 0.004 a.p.f.u. and 0.020 a.p.f.u., respectively. The analytical totals had a mean value of 98.84 wt. %. The crystals had rims richer in U and poorer in Th than the cores (Table S1).

The average chemical formula of uraninite from the altered granite was $\text{U}_{0.90}\text{Pb}_{0.05}\text{Th}_{0.02}\text{Fe}_{0.01}$, and the analytical totals ranged from 93.0 wt. % to 97.7 wt. % (Table 1). Some statistically significant differences ($p < 0.05$) were found between the concentrations of uraninite and other minerals from the altered and unaltered granite. The uraninite from the altered granite contained lower concentrations of U than the uraninite from fresh samples, ranging between 0.889–0.917 (1 s) a.p.f.u., and with a mean value of 0.903 a.p.f.u. The mean concentrations of Pb and Ca were also slightly lower than in unaltered uraninite (Table 1). Thorium (< 0.031 a.p.f.u.), Y (≤ 0.011 a.p.f.u.), LREE (≤ 0.002 a.p.f.u.), and HREE (≤ 0.003 a.p.f.u.) contents were similar in the uraninite from unaltered granite and altered granite. The altered uraninite, from the altered granite, had higher mean Si and F (0.023 a.p.f.u. and 0.060 a.p.f.u., respectively) concentrations than the unaltered uraninite (0.007 a.p.f.u. Si and 0.017 a.p.f.u. F). The mean Fe concentration of uraninite was lower in altered granite than in unaltered granite (0.011 a.p.f.u. and 0.020 a.p.f.u., respectively).

Table 1. Chemical compositions (in weight percent) and structural formula of uraninite, coffinite, and thorite from the unaltered and altered Variscan granites, Central Portugal.

	Uraninite				Coffinite		Thorite				
	Unaltered Granite		Altered Granite		Mean	σ	Unaltered Granite		Altered Granite		
	Mean	σ	Mean	σ			Mean	σ	Mean	σ	
Al ₂ O ₃	0.04	0.07	0.07	0.11	0.05	0.13	P ₂ O ₅	3.01	2.26	3.60	2.49
SiO ₂	0.14	0.16	0.51	0.40	16.00	1.64	SiO ₂	14.49	3.13	14.74	3.02
P ₂ O ₅	0.03	0.03	0.01	0.01	0.04	0.08	TiO ₂	0.15	0.13	0.10	0.09
CaO	0.09	0.10	0.03	0.09	0.90	0.83	ZrO ₂	0.41	0.25	0.22	0.39
ZrO ₂	0.04	0.02	0.02	0.03	0.06	0.19	HfO ₂	0.04	0.02	0.03	0.02
HfO ₂	0.02	0.05	—	—	—	0.01	ThO ₂	54.00	4.66	54.5	4.55
TiO ₂	—	—	—	—	—	—	UO ₂	3.56	3.06	4.41	3.84
Fe ₂ O ₃	0.52	0.62	0.30	0.41	0.29	0.47	Al ₂ O ₃	0.37	0.25	0.34	0.27
Y ₂ O ₃	0.25	0.14	0.40	0.10	0.18	0.25	Y ₂ O ₃	1.29	1.66	0.28	0.28
La ₂ O ₃	0.01	0.02	—	0.01	0.01	0.03	La ₂ O ₃	0.23	0.25	0.14	0.14
Ce ₂ O ₃	0.08	0.06	0.06	0.04	0.09	0.09	Ce ₂ O ₃	0.83	1.01	0.19	0.08
Pr ₂ O ₃	—	—	—	0.01	0.01	0.02	Pr ₂ O ₃	0.18	0.17	0.05	0.05
Nd ₂ O ₃	0.02	0.03	0.05	0.03	—	—	Nd ₂ O ₃	0.57	0.71	0.22	0.16
Sm ₂ O ₃	0.01	0.01	0.01	0.02	—	—	Sm ₂ O ₃	0.05	0.05	0.04	0.04
Gd ₂ O ₃	—	—	0.03	0.01	—	0.01	Gd ₂ O ₃	0.15	0.25	0.11	0.13
Dy ₂ O ₃	0.04	0.01	0.0	0.03	—	0.01	Dy ₂ O ₃	0.55	0.19	0.58	0.07
Ho ₂ O ₃	0.03	—	0.04	0.02	0.01	0.01	Ho ₂ O ₃	0.03	0.04	0.01	0.01
Er ₂ O ₃	0.01	0.01	0.01	0.01	0.01	0.01	Er ₂ O ₃	0.04	0.06	0.02	0.01
Yb ₂ O ₃	—	—	0.02	0.02	—	—	Yb ₂ O ₃	0.09	0.09	0.03	—
Lu ₂ O ₃	0.01	0.01	—	—	—	0.01	Lu ₂ O ₃	0.04	0.05	0.03	—
PbO	3.82	0.17	3.67	0.05	0.63	0.75	FeO	1.14	0.76	1.45	1.43
ThO ₂	1.57	0.55	1.51	0.83	0.61	0.96	CaO	1.92	0.56	2.07	0.92
UO ₂	91.98	1.76	89.57	1.31	76.56	5.17	PbO	0.79	1.03	1.42	1.23
F	0.12	0.22	0.42	0.11	0.34	0.06	F	0.40	0.30	0.37	0.55
Total	98.84	1.40	96.82	1.30	95.67	3.86	Total	84.35	4.09	87.96	3.008
Al	0.002	0.004	0.004	0.006	0.003	0.008	P	0.147	0.097	0.202	0.124
Si	0.007	0.007	0.023	0.018	0.933	0.071	Si	0.839	0.139	0.787	0.193
P	0.001	0.001	—	—	0.002	0.004	Ti	0.007	0.006	0.007	0.004
Ca	0.004	0.005	0.001	0.005	0.055	0.050	Zr	0.012	0.007	0.037	0.013
Zr	0.001	0.001	—	0.001	0.002	0.006	Hf	—	0.000	0.001	—
Hf	—	0.001	—	—	—	—	Th	0.710	0.129	0.660	0.082
Ti	—	—	—	—	—	—	U	0.046	0.045	0.033	0.050
Fe	0.020	0.023	0.011	0.016	0.014	0.024	Al	0.025	0.019	0.031	0.017
Y	0.006	0.004	0.010	0.002	0.006	0.008	Y	0.040	0.053	0.032	0.009
La	—	—	—	—	—	0.001	La	0.005	0.005	0.006	0.003
Ce	0.001	0.001	0.001	0.001	0.002	0.002	Ce	0.018	0.019	0.019	0.002
Pr	—	—	—	—	—	—	Pr	0.004	0.003	0.003	0.001
Nd	—	0.001	0.001	0.001	—	—	Nd	0.012	0.013	0.014	0.003
Sm	—	—	—	—	—	—	Sm	0.001	0.001	0.00	0.00
Gd	—	—	0.001	—	—	—	Gd	0.003	0.004	0.01	0.00
Dy	0.001	—	0.001	—	—	—	Dy	0.010	0.005	0.01	0.00
Ho	—	—	0.001	—	—	—	Ho	0.001	—	0.00	—
Er	—	—	—	—	—	—	Er	0.001	0.001	0.00	—
Yb	—	—	—	—	—	—	Yb	0.002	0.002	0.00	—
Lu	—	—	—	—	—	—	Lu	0.001	—	0.00	—
Pb	0.047	0.002	0.045	0.001	0.010	0.012	Fe	0.055	0.038	0.056	0.064
Th	0.016	0.006	0.016	0.009	0.008	0.013	Ca	0.119	0.033	0.150	0.051
U	0.927	0.022	0.903	0.014	0.995	0.075	Pb	0.012	0.015	0.012	0.019
F	0.017	0.030	0.060	0.016	0.060	0.023	F	0.074	0.080	0.07	0.09
Total	1.05	0.02	1.08	0.02	2.07	0.02	Total	2.142	0.0774	2.1433	0.1
	<i>n</i> = 13		<i>n</i> = 13		<i>n</i> = 14			<i>n</i> = 15		<i>n</i> = 17	

—: not detected. n.d.: not determined. Cation formula based on two atoms of oxygen for uraninite, and four atoms of oxygen for coffinite and thorite. n: number of analysis.

In general, therefore, uraninite from the altered granite was poorer in U, Fe, Pb, and Ca, and richer in Si and F. Locally, in the altered samples, uraninite was replaced by coffinite, and it had lower Th and Y contents, and similar U contents, to uraninite from the unaltered samples (Table S1, analyses 1 and 2).

Despite the small dimensions of uraninite grains, we could observe pattern zoning by an X-ray dot map obtained by the electron microprobe. The altered areas of uraninite crystals were relatively darker than unaltered areas, which was due to a relatively lower U content. In the altered granite, the uraninite grains had lower U contents in the rims than in the cores and, generally, the rims and alteration zones were poorer in U, Th, Pb, and Ce than in the cores (Table S1, Figure 4a).

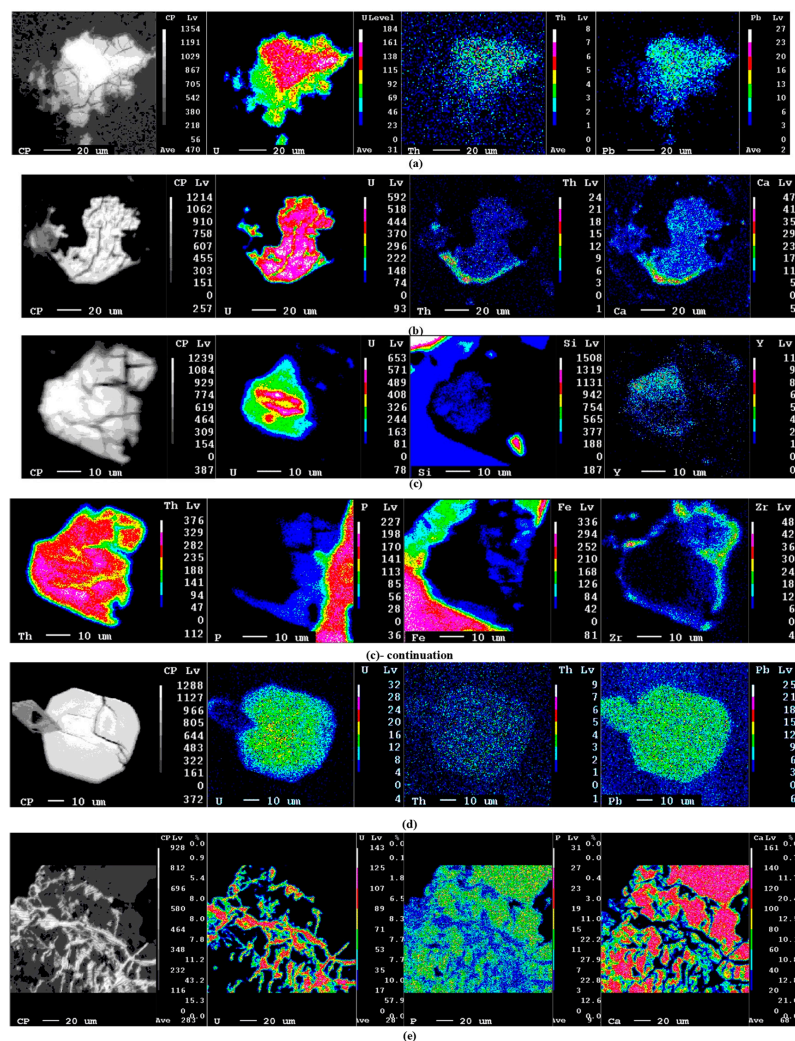


Figure 4. X-ray element maps, obtained by electron microprobe, of minerals from altered granite and hydrothermal quartz veins. (a) Altered crystal of uraninite from altered granite. (b) Altered crystal of coffinite from altered granite. (c) Altered crystal of thorite from altered granite. (d) Altered crystal of xenotime from altered granite. (e) Crystal of apatite from altered granite replaced by (meta)saleeite from hydrothermal quartz veins.

5.2. Coffinite

Chemical analyses of coffinite $[U(SiO_4)_{1-x}(OH)_{4x}]$ from altered granite are given in Table 1. Representative data for the chemical composition of coffinite are given in Supplementary Table S1. The characteristic feature of this coffinite is relatively variable concentrations of Si (0.824–1.049 a.p.f.u) and U (0.886–1.095 a.p.f.u). The amounts of Ca range from below the detection limit to 0.131 a.p.f.u (Table S1), with a mean concentration of 0.055 a.p.f.u (Table 1). The coffinite is poor in Y, P, and REE, particularly in HREE, with mean concentrations of $Y \leq 0.01$ a.p.f.u., $P \leq 0.002$ a.p.f.u., $(La + Ce + Pr + Nd + Sm) \leq 0.002$ a.p.f.u., and $(Gd + Dy + Ho + Er + Yb + Lu) \leq 0.001$ a.p.f.u. Thorium and Pb contents are also low, reaching 0.008 a.p.f.u. and 0.010 a.p.f.u., respectively. The analytical totals range from 89.75 wt. % to 100.73 wt. %, probably due to different degrees of hydration (Table 1 and Table S1).

Backscattered electron (BSE) images and X-ray element maps showed clear differences between the rims and cores of coffinite, reflecting an enrichment in Th, Ca, Pb, Zr, and a depletion in U in the crystal rims (Table S1, Figure 4b). Coffinite intergrowths with thorite were not found, but some coffinite grains replaced uraninite.

5.3. Thorite

Thorite [(Th,U)SiO₄] was found in all of the granite samples (Table 1), and its composition was variable in all of them, even within the grains (Table S2, in Supplementary file). This variability is also noted by [13]. Thorite occurs as very fine-grained crystals (~10 μm), and forms intergrowths with large amounts of associated minerals, such as xenotime, monazite, apatite, and zircon (Figure 3e–i). The composition of thorite is dominated by the major components Th and Si. Thorium concentrations of thorite were similar in unaltered and altered granite, but had a higher variability in altered granite (Tables 1 and S2). Thorium contents ranged between 44.95–60.75 wt. % ThO₂ in the unaltered granite, and between 39.97–68.97 wt. % ThO₂ in the altered granite (Table S2). The same observation could be made for the SiO₂ wt. % contents, ranging from 7.37 to 17.69 in the thorite from the unaltered granite, and from 8.18 to 18.07 in the altered granite (Table S2). The analytical totals were low either in thorite from the unaltered granite or the altered granite (Table 2), which could be due to some hydration.

The mean U, Y, P, REE, Fe, Ca, Pb, and F contents of the thorite from the altered granite were similar to those of the thorite from the unaltered granite (Table 1 and Table S2). The UO₂ wt. % concentrations in thorite ranged from 0.45 to 8.63 in the unaltered granite, and from 0.46 to 10.43 in the altered granite (Table S2). The Y₂O₃ wt. % concentrations ranged from 0.01 to 5.62 in the unaltered granite, and from 0.07 to 4.20 in the altered granite (Table S2).

In the altered granite, thorite filled the fractures of other minerals, such as apatite, monazite, and biotite, mainly in their rims (Figure 2e–i), and seemed to replace monazite along fractures that were associated with xenotime (Figure 3i). A zoned crystal of thorite was analyzed (crystal B in Table S2) in the altered granite, and the darker rim was poorer in Si, U, Y, Ca, and REE, and richer in P, Th, Fe, Pb, and F, than the respective lighter core (Table S2).

Figure 4c presents an X-ray map of a fractured thorite grain from the most altered granite (crystal A, Table S2) that is close to the fractures. The crystals are more altered and darker than in the areas away from those fractures, which may be due to decreased U contents. The most altered areas close to the fractures are clearly poorer in U and Si (0.46–3.87 wt. % UO₂ and 9.95–12.99 wt. % SiO₂) than the areas away from the fractures (7.23–10.43 wt. % UO₂ and 16.03–16.45 wt. % SiO₂) (Table S2 and Figure 4c). These most altered areas are richer in P, Fe, Pb, F and Zr than the unaltered areas (Table S2). Thus, the altered thorite is the poorest in U and Si, and the richest in P, Fe, Pb, and F, in its rims and close to the fractures. The distribution of Zr is not homogeneous in the most altered areas (such as that of Pb), but Zr seems to surround thorite crystal (Figure 4c).

5.4. Zircon

Chemical compositions of zircon (ZrSiO₄) from unaltered granite and mineralized quartz veins were presented by [15]. Zircon compositions from the altered granite and new analyses of zircon from the mineralized quartz veins are given in Table 2, and analyses of zircon grain core and rims are given in supplementary Table S3. In general, the zircon from unaltered granite had the lowest mean Fe, P, U, and Pb content (0.20 wt. % Fe₂O₃, 0.12 wt. % P₂O₅, 0.05 wt. % UO₂, and 0.07 wt. % PbO), and the highest mean Zr and Hf content (65.24 wt. % ZrO₂, 1.42 wt. % HfO, Table 2 and [15]). In general, the zircon from altered granite had the highest mean of P (0.40 wt. % P₂O₅), Y (0.55 wt. % Y₂O₃), U (0.22 wt. % UO₂), La + Ce (0.28 wt. % REE₂O₃), and Pb (0.23 wt. % PbO), and the lowest mean analytical totals for Si and Zr (30.56 wt.% SiO₂, 61.29 wt. % ZrO₂). Meanwhile, the mean Hf concentration was similar to that of the zircon from mineralized quartz veins (Tables 2 and S3). In unaltered granite, zircon did not present significant chemical variation either within grains or between grains, but the distribution of U in hydrothermally altered grains showed a chemical zonation, and the rims contained more U (up to 0.62 wt. % UO₂) than the cores (Table 3). However, some altered crystals presented an inverse zonation, with a loss of U in the rims (Table 3). The zircon from mineralized quartz veins had the highest mean contents of Mg (0.14 wt. % MgO) and 0.13 wt. % UO₂, but very high values of U (~15 wt. % UO₂) were found in the rims of some dissolved and altered crystals (Table S3). These rims with high U contents had very low contents of SiO₂ (~18 wt. %), ZrO₂ (~43 wt. %), and analytical totals (~89 wt. %),

and very high values of P₂O₅ (~3 wt. %) and Fe₂O₃ (1.3 wt. %) (Table S3). Therefore, the numbers of cations per chemical formula were not calculated. The composition of the respective unaltered cores was close to [(Zr,Hf)SiO₄], and the U contents were similar to those found in the zircon from altered granite (Table S3). Cabral Pinto et al. [15] also presented values of UO₂ (~18 wt. %), Fe₂O₃ (~8 wt. %), SiO₂ (~14 wt. %), and ZrO₂ (41 wt. %) in the rims of very altered zircon crystals.

Table 2. Chemical composition (in weight percent) and structural formula of zircon and xenotime from the Variscan unaltered and altered granites, and associated hydrothermal quartz veins, Central Portugal.

	Zircon						Xenotime						
	Unaltered Granite		Altered Granite		Quartz Veins		Unaltered Granite		Altered Granite		Quartz Veins		
	Mean	σ	Mean	σ	Mean	σ	Mean	σ	Mean	σ	Mean	σ	
SiO ₂	31.50	0.89	30.56	1.14	34.15	1.78	P ₂ O ₅	33.68	0.56	34.02	0.38	32.85	0.75
ZrO ₂	65.24	2.78	61.29	3.21	61.74	1.54	SiO ₂	0.79	0.20	0.71	0.16	n.d.	n.d.
HfO ₂	1.42	0.23	1.31	0.37	1.31	0.21	TiO ₂	—	—	—	—	n.d.	n.d.
TiO ₂	0.01	0.02	0.03	0.02	0.05	0.07	ZrO ₂	—	—	—	—	0.06	0.16
Al ₂ O ₃	0.04	0.17	0.31	0.43	0.24	0.27	HfO	0.24	0.02	0.26	0.02	—	—
Fe ₂ O ₃	0.20	0.16	0.30	0.19	0.31	0.29	ThO ₂	0.15	0.10	0.13	0.09	0.44	0.21
MgO	0.02	0.07	0.07	0.13	0.14	0.04	UO ₂	2.35	0.49	1.57	0.39	0.45	0.37
MnO	0.02	0.03	0.04	0.03	0.04	0.03	Y ₂ O ₃	38.90	0.29	39.29	0.60	43.49	1.01
WO ₃	0.05	0.10	0.11	0.10	0.07	0.05	La ₂ O ₃	—	—	—	—	—	—
K ₂ O	0.01	0.02	0.02	0.02	0.12	0.12	Ce ₂ O ₃	0.06	0.02	0.03	0.03	0.04	0.03
Y ₂ O ₃	0.12	0.23	0.55	0.30	0.32	0.42	Pr ₂ O ₃	0.01	0.01	0.01	0.01	0.05	0.07
La ₂ O ₃	0.10	0.09	0.14	0.08	0.04	0.03	Nd ₂ O ₃	0.37	0.05	0.35	0.04	0.12	0.03
Ce ₂ O ₃	0.07	0.13	0.14	0.14	0.05	0.03	Sm ₂ O ₃	0.63	0.05	0.64	0.11	0.53	0.09
CaO	0.07	0.24	0.36	0.51	0.05	0.13	Eu ₂ O ₃	n.d.	n.d.	n.d.	n.d.	0.29	0.10
PbO	0.07	0.11	0.23	0.16	0.15	0.11	Gd ₂ O ₃	1.91	0.15	2.00	0.35	3.27	0.58
UO ₂	0.05	0.11	0.22	0.15	0.13	0.21	Tb ₂ O ₃	n.d.	n.d.	n.d.	n.d.	0.85	0.07
ThO ₂	0.05	0.07	0.08	0.09	0.06	0.06	Dy ₂ O ₃	5.47	0.35	5.51	0.55	6.54	0.13
P ₂ O ₅	0.12	0.14	0.40	0.21	0.17	0.17	Ho ₂ O ₃	1.07	0.03	1.11	0.04	2.74	0.22
Total	99.16	2.89	96.17	3.31	99.16	2.38	Er ₂ O ₃	2.34	0.28	2.36	0.43	3.61	0.17
							Tm ₂ O ₃	n.d.	n.d.	n.d.	n.d.	0.50	0.06
Si	3.927	0.056	3.922	0.068	4.185	0.110	Yb ₂ O ₃	3.14	0.25	3.10	0.44	2.74	0.26
P	0.013	0.014	0.043	0.022	—	—	Lu ₂ O ₃	0.67	0.03	0.64	0.06	0.93	0.08
Al ^{iv}	0.006	0.013	0.047	0.033	0.035	0.038	FeO	0.13	0.04	0.11	0.07	n.d.	n.d.
Σ	3.945	0.053	4.01	0.05	4.220	0.112	CaO	0.28	0.06	0.24	0.05	n.d.	n.d.
Al ^{vi}	—	0.020	—	0.067	—	—	PbO	0.15	0.06	0.15	0.07	n.d.	n.d.
Zr	3.966	0.074	3.835	0.085	3.690	0.106	F	0.02	0.02	0.03	0.04	n.d.	n.d.
Hf	0.051	0.008	0.048	0.014	0.046	0.010	Total	92.36	0.85	92.23	0.80	99.48	0.66
Fe ³⁺	0.019	0.017	0.029	0.020	0.028	0.028							
Mg	0.004	0.013	0.013	0.024	0.026	0.012	P	4.021	0.044	4.044	0.03	3.845	0.041
Ti	0.001	0.002	0.003	0.002	0.001	0.001	Si	0.111	0.027	0.100	0.02	n.d.	n.d.
Pb	0.002	0.004	0.008	0.006	0.005	0.003	Ti	—	—	—	—	n.d.	n.d.
U	0.001	0.003	0.006	0.005	0.004	0.005	Zr	—	—	—	—	0.004	0.010
Th	0.001	0.002	0.002	0.003	0.002	0.002	Hf	0.011	0.001	0.012	0.001	—	—
Y	0.008	0.015	0.038	0.020	0.029	0.017	Th	0.005	0.003	0.004	0.003	0.014	0.007
La	0.004	0.004	0.005	0.003	0.002	0.001	U	0.074	0.015	0.049	0.012	0.014	0.011
Ce	0.003	0.003	0.003	0.003	0.001	0.001	Y	2.920	0.020	2.935	0.027	3.200	0.059
Ca	0.009	0.036	0.049	0.075	0.007	0.015	La	—	—	—	—	—	—
Σ	4.07	0.06	4.04	0.07	3.830	0.113	Ce	0.003	0.001	0.002	0.002	0.002	0.002
N	n = 72		n = 20		n = 55		Pr	—	—	—	0.001	0.003	0.004
							Nd	0.018	0.002	0.018	0.002	0.006	0.001
							Sm	0.030	0.003	0.031	0.01	0.025	0.005
							Eu	n.d.	n.d.	n.d.	n.d.	0.014	0.005
							Gd	0.089	0.008	0.093	0.017	0.150	0.028
							Tb	n.d.	n.d.	n.d.	n.d.	0.038	0.003
							Dy	0.248	0.018	0.249	0.026	0.291	0.008
							Ho	0.048	0.001	0.050	0.002	0.120	0.011
							Er	0.140	0.016	0.141	0.025	0.212	0.008
							Tm	n.d.	n.d.	n.d.	n.d.	0.022	0.003
							Yb	0.135	0.010	0.133	0.018	0.116	0.011
							Lu	0.029	0.001	0.027	0.002	0.039	0.003
							Fe	0.016	0.005	0.013	0.009	n.d.	n.d.
							Ca	0.042	0.009	0.035	0.008	n.d.	n.d.
							Pb	0.006	0.002	0.006	0.003	n.d.	n.d.
							F	0.008	0.009	0.013	0.016	n.d.	n.d.
							Total	7.96	0.025	7.95	0.008	8.09	0.027
								n = 7		n = 9		n = 6	

—: not detected. n.d.: not determined. Cation formula based on 16 atoms of oxygen for both zircon and xenotime. n: number of analysis.

5.5. Xenotime

The chemical analyses of xenotime (YPO₄) are presented in Table 2. There was no significant difference between the chemical composition of xenotime from the unaltered and altered granites,

except for the U content, which was lower (mean of 1.57 wt. % UO_2) in the xenotime from the altered granite. In contrast, it had a mean of 2.35 wt. % UO_2 in the xenotime from the unaltered granite (Table 2). The rims of the xenotime crystals from the altered granite were poorer in U than the respective cores (Figure 4d, Table S3).

The xenotime from the mineralized quartz veins was poorer in P, U, and Nd, and richer in Y, Th, Gd, Dy, Ho, Er, and Lu than the xenotime from the unaltered and altered granites (Table 2). The xenotime from the mineralized quartz veins had a mean content of 0.45 wt. % UO_2 and 43.49 wt. % Y_2O_3 , but a value of 1.02 wt. % UO_2 occurred in the rims of the altered crystals (Table 2).

The HREE were 0.690–0.692 a.p.f.u. in the xenotime from the unaltered and altered granites, and 0.980 a.p.f.u. in the xenotime from the mineralized quartz veins. The LREE were low: 0.050–0.053 a.p.f.u. in the xenotime from the unaltered and altered granites, and 0.035 a.p.f.u. in the xenotime from the quartz veins (Table 2). Hafnium, Fe, Ca, and Pb were detected in the xenotime from the granites, but were not found in the xenotime from the mineralized quartz veins (Table 2). Thorium contents were similar in the xenotime from all of the granite samples, but slightly higher Th contents were found in the xenotime from the quartz veins (Table 2).

5.6. Monazite

The chemical composition of Ce-monazite ($\text{Ce, La, Nd, Th})\text{PO}_4$ from the unaltered granite are presented in Table 3. The chemical composition of monazite in the altered granite was more variable than in the unaltered granite, and had generally higher mean contents of Si and Al, and lower mean contents of U (0.77 wt. % U_3O_8), Ca, Th (6.84 wt. % ThO_2), and F (0.20 wt. % F) than Ce-monazite from the unaltered granite (1.26 wt. % U_3O_8 , 0.27 wt. % F, and 7.91 wt. % ThO_2 , Table 3).

The Ce-monazite from the mineralized quartz veins was poorest in Ca, Y, Th, and U, and richest in Si, Fe, LREE, and F (Table 3). It had mean concentrations of 0.19 wt. % U_3O_8 and 1.14 wt. % ThO_2 , and a low analytical total (Table 3).

5.7. Apatite

Chemical analyses of apatite [$\text{Ca}_{10}(\text{PO}_4)_6(\text{OH,F,Cl})_2$] from the granite and related hydrothermal quartz veins are given in Table 3. They are F-apatites. In the altered granite and mineralized quartz veins, the apatite grains were vacuolated, and showed a high porosity (Figures 3f–h and 4e), indicating apatite dissolution. The apatite from the altered granite generally had higher mean contents of Fe, Mg, K, Si, Al, Th, Y, La, and Ce, and lower mean contents of Mn, Ca, Na, P, U, and F, and lower analytical totals, than the apatite from the unaltered granite. However, analytical variability was higher in the apatite from the altered granite (Table 3). The apatite from the hydrothermal quartz veins had mean contents of Ca and P that were similar to the apatite from the unaltered granite, but higher mean contents of U and F (0.13 wt. % UO_2 , and 2.76 wt. % F). Meanwhile, Y, La, and Ce were not detected in this apatite (Table 3). Apatite crystals from the mineralized quartz veins that were associated with uranium–phosphate phases had the highest U (1.09 wt. % UO_2) content (crystal A in Table 3 and Figure 4e). This apatite was richer in Fe, and poorer in P than the apatite that was not associated with uranium–phosphate phases.

5.8. Saleeite and Meta-Saleeite

The chemical compositions of saleeite and meta-saleeite ($\text{Mg, Fe}^{2+})(\text{UO}_2)_2(\text{PO}_4)_2 \cdot 4\text{H}_2\text{O}$ from the hydrothermal quartz veins are presented in Table 4. Some U-phosphates were associated with apatite (Figure 3j and the X-ray map in Figure 4e), while others were not (Figure 3l). In general, the uranium phosphates that were associated with apatite had lower FeO and higher MgO and CaO than those that were not associated with apatite. However, crystals with high Fe contents were also found in the (meta)saleeite that was associated with apatite (Table 4).

Table 3. Chemical composition (in weight percent) and structural formula of monazite and apatite from the Variscan unaltered and altered granites, and associated hydrothermal quartz veins, Central Portugal.

	Monazite						Apatite								
	Granite		Quartz Veins				Granite		Quartz Veins						
	Unaltered Granite		Altered Granite		Unaltered Granite		Altered Granite		Unaltered Granite		Altered Granite		Quartz Veins		Crystal A
	Mean	σ	Mean	σ	Mean	σ	Mean	σ	Mean	σ	Mean	σ	Mean	σ	
P ₂ O ₅	29.44	0.73	30.06	0.84	28.54	1.41	FeO	0.51	0.25	0.66	0.50	0.40	0.33	0.55	
SiO ₂	0.20	0.13	0.37	0.32	0.41	0.50	MnO	0.55	0.15	0.08	0.09	0.03	0.03	n.d.	
Ce ₂ O ₃	25.33	1.47	25.84	1.31	29.99	1.18	MgO	0.03	0.02	0.21	0.22	0.09	0.04	0.19	
La ₂ O ₃	10.45	1.05	11.08	0.89	13.47	1.92	CaO	52.28	1.73	49.25	2.07	53.19	0.59	53.98	
Nd ₂ O ₃	10.84	0.58	10.85	0.86	13.21	1.53	SrO	0.03	0.03	0.04	0.02	n.d.	n.d.	n.d.	
Pr ₂ O ₃	2.57	0.51	2.63	0.20	2.64	0.77	Na ₂ O	0.11	0.04	0.05	0.04	0.01	—	0.01	
Sm ₂ O ₃	1.68	1.18	—	—	1.65	1.07	K ₂ O	0.04	0.04	0.21	0.13	—	—	—	
Gd ₂ O ₃	2.86	0.32	3.04	0.29	n.d.	n.d.	P ₂ O ₅	41.17	0.48	36.82	2.69	41.39	1.34	38.47	
Dy ₂ O ₃	0.91	0.21	0.67	0.14	n.d.	n.d.	SiO ₂	0.16	0.20	1.56	1.00	—	—	—	
Ho ₂ O ₃	—	—	—	—	n.d.	n.d.	TiO ₂	—	0.01	0.02	0.03	0.01	0.02	n.d.	
Er ₂ O ₃	—	—	—	0.01	n.d.	n.d.	Al ₂ O ₃	0.05	0.09	0.56	0.29	0.04	0.07	0.04	
Yb ₂ O ₃	—	0.01	—	—	n.d.	n.d.	BaO	—	—	—	—	n.d.	n.d.	n.d.	
Lu ₂ O ₃	0.07	0.03	0.05	0.02	n.d.	n.d.	PbO	0.01	0.03	—	—	—	—	0.01	
Fe ₂ O ₃	0.07	0.12	0.08	0.15	0.46	1.09	UO ₂	0.01	0.01	—	0.01	0.13	0.09	1.09	
CaO	1.73	0.30	1.42	0.31	0.24	0.17	ThO ₂	0.01	0.01	0.56	0.48	—	—	—	
PbO	0.18	0.13	0.17	0.08	0.03	0.07	Y ₂ O ₃	0.29	0.07	0.47	0.23	—	—	—	
Al ₂ O ₃	0.05	0.11	0.14	0.16	0.13	0.32	La ₂ O ₃	0.04	0.06	0.31	0.25	—	—	0.02	
Y ₂ O ₃	2.14	0.75	2.38	0.52	0.57	0.29	Ce ₂ O ₃	0.11	0.06	0.52	0.30	—	—	0.02	
ThO ₂	7.91	1.01	6.84	0.73	1.14	0.98	F	2.24	0.30	2.08	0.47	2.76	0.13	2.62	
U ₃ O ₈	1.26	0.53	0.77	0.56	0.19	0.10	Cl	0.02	0.02	0.01	0.01	0.01	0.01	0.01	
ZrO ₂	0.01	0.01	0.02	0.02	n.d.	n.d.	Total	97.67	1.97	93.42	2.75	98.06	1.49	97.01	
HfO	0.02	0.01	0.01	0.01	n.d.	n.d.	O≡F	0.95	0.88	—	—	1.16	—	1.10	
MgO	n.d.	n.d.	n.d.	n.d.	0.01	0.02	O≡Cl	—	—	—	—	—	—	n.d.	
F	0.27	0.17	0.20	0.12	0.43	0.18	Total	96.72	—	92.55	—	96.90	—	95.91	
Total	97.99	1.75	96.62	3.42	93.11	2.11									
O≡F	0.12	0.07	0.08	0.05	0.18	—	P	5.883	0.063	5.628	0.212	5.859	0.093	5.629	
Total	97.88	1.75	96.54	3.45	92.93	—	Si	0.028	0.034	0.282	0.184	—	—	—	
							Σ	5.91	0.06	5.91	—	5.86	0.09	5.63	
P	3.952	0.037	4.012	0.040	4.029	0.106	Al	0.009	0.017	0.120	0.061	0.008	0.014	0.007	
Si	0.032	0.021	0.059	0.053	0.068	0.081	Mg	0.008	0.006	0.056	0.060	0.022	0.011	0.049	
P + Si	3.98	—	4.07	—	4.10	—	Fe	0.072	0.035	0.099	0.076	0.056	0.046	0.080	
Ce	1.470	0.098	1.492	0.072	1.831	0.080	Mn	0.078	0.021	0.012	0.013	0.004	0.004	n.d.	
La	0.611	0.069	0.645	0.058	0.828	0.115	Na	0.037	0.012	0.018	0.015	0.003	0.001	0.003	
Nd	0.614	0.032	0.611	0.036	0.787	0.104	K	0.008	0.008	0.049	0.029	—	—	—	
Pr	0.148	0.030	0.151	0.009	0.160	0.047	Ca	9.453	0.182	9.525	0.431	9.529	0.193	9.996	
Sm	0.092	0.065	—	—	0.095	0.061	Sr	—	—	—	—	n.d.	n.d.	n.d.	
Gd	0.150	0.068	0.159	0.013	n.d.	n.d.	Ba	—	—	—	—	n.d.	n.d.	n.d.	
Dy	0.046	0.021	0.034	0.006	n.d.	n.d.	Pb	0.001	0.001	—	—	—	—	—	
Ho	—	—	—	—	n.d.	n.d.	U	—	—	—	—	0.005	0.010	0.042	
Er	—	—	—	—	n.d.	n.d.	Th	—	—	0.023	0.020	—	—	—	
Yb	—	—	—	—	n.d.	n.d.	Σ	9.67	0.23	9.90	0.50	9.63	0.23	10.18	
Lu	0.003	0.002	0.002	0.001	n.d.	n.d.	F	1.198	0.157	1.187	0.292	1.457	0.139	1.43	
Fe	0.008	0.014	0.009	0.018	0.058	0.135	Cl	0.007	0.006	0.003	0.004	0.002	0.002	0.002	
Ca	0.294	0.051	0.240	0.048	0.043	0.030	OH	0.795	0.158	0.810	0.293	0.541	0.072	0.568	
Pb	0.008	0.006	0.007	0.003	0.001	0.003	n = 27			n = 14		n = 16			
Al	0.009	0.020	0.026	0.029	0.026	0.061									
Y	0.181	0.062	0.200	0.040	0.051	0.026									
Th	0.285	0.039	0.245	0.024	0.043	0.037									
U	0.043	0.018	0.026	0.018	0.007	0.004									
Zr	0.001	0.001	0.001	0.001	n.d.	n.d.									
Hf	0.001	—	0.001	—	n.d.	n.d.									
Mg	n.d.	n.d.	n.d.	n.d.	0.002	0.006									
F	0.135	0.088	0.097	0.066	0.094	0.021									
Total	4.10	—	3.95	—	3.93	—									
	n = 18		n = 12		n = 23										

—: not detected. n.d.: not determined. Cation formula based on 16 atoms of oxygen for monazite, and 25 atoms of oxygen for apatite. n: number of analysis.

Table 4. Chemical composition (in weight percent) and structural formula of saleeite and meta-saleeite from the hydrothermal quartz veins, Central Portugal.

U-Phosphates								
Mineralized Quartz Veins								
Associated with Apatite								
	Meta-Saleeite		Saleeite		Meta-Saleeite		Saleeite	
	Mean	σ	Mean	σ	Mean	σ	Mean	σ
FeO	0.72	0.38	0.77	0.75	0.82	0.53	0.95	0.71
MnO	0.01	0.01	—	—	—	—	0.04	0.06
MgO	4.27	0.24	4.32	0.20	4.22	0.29	4.16	0.32
TiO ₂	0.03	0.03	0.05	0.05	0.05	0.04	0.03	0.02
CaO	0.69	0.26	0.80	0.24	0.07	0.05	0.13	0.08
ZnO	n.d.	n.d.	n.d.	n.d.	0.18	0.03	0.23	0.03
Y ₂ O ₃	n.d.	n.d.	n.d.	n.d.	0.01	0.01	0.02	0.04
PbO	0.05	0.08	0.01	0.01	0.10	0.13	0.02	0.03
ThO ₂	0.01	0.01	0.01	0.01	—	0.01	0.03	0.05
UO ₂	60.39	2.04	58.74	2.32	61.48	0.87	59.88	1.24
La ₂ O ₃	0.01	0.01	0.01	0.01	0.03	0.04	—	—
Ce ₂ O ₃	0.03	0.04	—	—	0.02	0.03	0.03	0.03
Na ₂ O	n.d.	n.d.	n.d.	n.d.	0.08	0.17	0.04	0.04
K ₂ O	n.d.	n.d.	n.d.	n.d.	0.06	0.07	0.01	0.02
SiO ₂	0.06	0.08	0.01	0.02	0.47	0.37	0.23	0.26
Al ₂ O ₃	0.15	0.07	0.24	0.14	0.04	0.05	0.13	0.10
P ₂ O ₅	16.91	0.88	15.53	0.51	15.92	0.23	15.14	0.63
F	0.46	0.14	0.48	0.09	n.d.	n.d.	n.d.	n.d.
Total	83.79	1.01	80.95	0.59	83.42	0.94	81.07	1.85
Fe	0.084	0.046	0.097	0.098	0.099	0.063	0.124	0.086
Mn	0.001	0.001	—	—	—	—	0.005	0.006
Mg	0.885	0.071	0.979	0.054	0.901	0.071	0.967	0.080
Ti	0.003	0.004	0.005	0.005	0.006	0.004	0.004	0.002
Ca	0.102	0.035	0.130	0.043	0.010	0.008	0.021	0.013
Zn	n.d.	n.d.	n.d.	n.d.	0.039	0.020	0.054	0.028
Y	n.d.	n.d.	n.d.	n.d.	0.001	0.001	0.002	0.003
Pb	0.002	0.003	—	—	0.004	0.005	0.001	0.001
Th	—	—	—	—	—	—	0.001	0.002
U	1.869	0.161	1.988	0.129	1.961	0.061	2.080	0.058
La	—	—	—	—	0.002	0.002	—	—
Ce	0.001	0.002	—	—	0.001	0.001	0.002	0.002
Na	n.d.	n.d.	n.d.	n.d.	0.022	0.047	0.012	0.011
K	n.d.	n.d.	n.d.	n.d.	0.010	0.014	0.002	0.004
Si	0.008	0.011	0.001	0.003	0.068	0.050	0.036	0.039
Al	0.025	0.011	0.043	0.025	0.007	0.008	0.024	0.018
P	1.992	0.011	1.999	0.003	1.932	0.050	2.000	0.039
H ₂ O	8	—	10	—	8	—	10	—
P + Si	2.00	—	2.00	—	2.00	—	2.00	—
Σ	1.07	—	1.21	—	1.01	—	1.12	—
U	1.87	—	1.99	—	1.96	—	2.08	—
	<i>n</i> = 10	—	<i>n</i> = 8	—	<i>n</i> = 12	—	<i>n</i> = 12	—

—: not detected. n.d.: not determined. Cation formula based on two atoms of P (+Si) for saleeite and meta-saleeite, Σ = Fe + Mn + Mg + Ca + Y + Na + K. *n*: number of analysis.

6. Discussion

Uraninite is the main host of uranium in unaltered peraluminous biotite granite, which has a molecular ratio of Al₂O₃/(CaO + Na₂O + K₂O) ranging from 1.08 to 1.16 [28]. In peraluminous granites, uraninite is the host of considerable bulk-rock uranium content [11], and is the most important uranium mineral in terms of abundance, occurrence, and economic value [4]. The disposal of UO₂ from used nuclear fuel is an environmental issue, and the studies of stability, alteration, and leaching of uraninite are numerous [30–43].

Under oxidizing conditions, uraninite gives rise to many complex uranyl minerals, such as carbonates (e.g., bijvoetite, urancalcarite, znucalite, etc.), silicates (e.g., coffinite, sklodowskite, soddyite, swamboite), phosphates (e.g., yingjiangite, autunite and meta-autunite, saleeite, metasaleeite, etc.), oxyhydroxides (e.g., clarkeite, ianthinite, vandendriesscheite, etc.), vanadates (e.g., carnotite, curiënite, etc.), molybdates (e.g., calcurmolite, cousinite, etc.), arsenates, etc. [4,14,18].

Uraninite occurs mainly in unaltered granite and is magmatic [15]; it is rare in altered granite, and was not found in mineralized quartz veins. In unaltered granite, some uraninite crystals were zoned with rims enriched in U and poorer in Th than the cores (Table 1), which reflected the Th–U substitutions. Uraninite from the unaltered granite was richer in U, Pb, Ca, and Fe, and poorer in Si and F than the uraninite from the altered granite (Table 1). In the altered granite, uraninite showed fractures and vacuoles, and had radioactive damage halos filled with late pyrite, U–S-bearing phases, and Fe oxyhydroxides (Figure 3a–c). The analytical totals of uraninite were lower in the altered granite than in the unaltered granite (Table 1). The crystal rims of uraninite from the altered granite were poorer in U than the respective cores, as well as both the rims and cores of the zoned uraninite crystals from the unaltered granite (Table S1 and Figure 4a). Locally, in the altered granite, uraninite was replaced by coffinite, but the U contents of this uraninite were similar to that of the altered uraninite (Table S1, analyses 1, 2). In general, hydrothermal alteration caused a decrease in U, Pb, Ca, and Fe, and an increase in Si and F in uraninite (Table 1), indicating uranium removal from the crystal rims and alteration zones, and the formation of coffinite.

Coffinite $U[SiO_4]_{1-x}(OH)_{4x}$ [14] is a tetragonal orthosilicate with a zircon-type structure. The U–Th silicates thorite and coffinite are usually metamitic and can incorporate molecular H_2O , and the formula $(U,Th)SiO_4 \cdot nH_2O$ ($n < 4$) used by various authors (e.g., [4,44–47]) is equally valid [14]. According to [4], U–Th silicates form two series of anhydrous and hydrated minerals with the chemical formulas: $(U,Th)SiO_4$ and $(U,Th)SiO_4 \cdot nH_2O$ ($n < 4$). The hydrated U(IV)-silicate, coffinite, was only found in the most altered granite, and some crystals replaced uraninite. So, coffinite resulted from uraninite alteration, since uraninite is unstable in supergenic and hydrothermal environments [14]. The lower analytical totals found in analyzed coffinite (Table 1) were probably due to the presence of OH or H_2O , as there were coffinite analyses close to 100%, and all of the analyses were performed with the same analytical procedures. The analyzed coffinite was close to the end member $USiO_4$. Coffinite crystals with a compositional heterogeneous core–rim were observed, with a depletion in U in the crystal rims, lower UO_2 contents up to 10 wt. % relative to the respective cores, and enrichment in Th and Ca in the crystal rims (Table S1 and Figure 4b). The low U contents (0.924 a.p.f.u. and 0.886 a.p.f.u.) found in the crystal rims might have been due to meteoric alteration, and indicated uranium mobilization from coffinite.

Thorite was widespread in the unaltered and altered granites. Thorite seemed to be magmatic in the unaltered granite (Figure 3e), but secondary thorite was found in the altered granite, which was related to the chloritization of biotite, and alteration of apatite (Figure 3g) and plagioclase. Locally, it was zoned (Figure 4c and Table 1 and Table S2), and occurred associated with zircon, but the textural relation did not reveal whether it was a product of zircon alteration, as found by [48]. In the altered granite, thorite replaced apatite (Figure 3g) and monazite (Figure 3h,i). It was associated with xenotime, and filled fractures of biotite.

Thorite composition was variable (Table 1 and Table S2), which agrees with [44,49]. The analytical totals were low (Table 1), but the analyses were close to stoichiometry (totals of 2.14 a.p.f.u., Table 1). These low totals could probably be attributed to hydration, because thorite is highly metamitic. However, they were not due to the presence of elements not included in the list, because the scanning of the peaks by EDS did not show them. The high contents of Fe, Ca, Zr, and P can indicate some analytical interferences [49], because thorite occurs as very small crystals associated with zircon and xenotime, and replaces monazite and apatite (Table 1 and 2, and Table S2, Figure 3f–i), whereas the high contents of Y and Zr may suggest a solid solution with xenotime and zircon [49]. Thorite forms a solid solution with coffinite [49], but the coffinite analyzed was almost pure $USiO_4$. The uranium contents in the thorite ranged from 0.45 wt. % UO_2 to 10.43 wt. % UO_2 (Table 1 and Table S2). The uranium, Y, P, REE, Fe, Ca, Pb, and F contents were not significantly different in the thorite from the unaltered and altered granites, so it seems that there was no significant difference in the chemical composition of the thorite from these granites. However, in the thorite from the unaltered granite, there was a regular decrease in the U content with increasing P content, and an enrichment of (Y+HREE) relative to LREE,

as found by [16], but they were not found in the thorite from the altered granite. Thus, there were two generations of thorite: the first was primary and belonged to the unaltered granite, and the second resulted from the alteration of other minerals such as monazite and apatite. In the altered granite, the zoned crystals of thorite had rims that were poorer in U, Si, Y, Ca, and REE, and richer in P, Th, Fe, Pb, and F, than the respective cores; also, in the altered zones close to the fractures, the thorite was poorer in U and Si and richer in P, Fe, Pb, and F than in the unaltered zones (Table 1, Table S2 and Figure 4c). So, U and Si were mobilized from thorite in its rims and fracture zones.

Ce-monazite is a primary mineral, or it can be formed by the metasomatic alteration of apatite (Figure 3h), which is also documented in the literature [49–52]. Elsewhere, it has been replaced by thorite (Figure 3i). The replacement of monazite by thorite was reported by [16,53,54], and a high huttonite (ThSiO_4) component was found in altered monazite. The textural evidence found in altered granite indicates that some monazite was formed by apatite alteration, and in turn, some thorite was formed from monazite and apatite alteration.

Ce-monazite from the altered granite was poorer in U, Ca, Th, and F, and richer in Si and Al than the Ce-monazite from the unaltered granite (Table 3); so, hydrothermal alteration of the granite caused the removal of U, Th, F, and Ca from the monazite. Altered monazite has a pervasive porosity (Figure 3i) and was replaced by thorite, but uraninite was not found in this altered monazite, as reported by [16], due to the oxidizing conditions of the hydrothermal fluid. So, some Th was incorporated in thorite, which precipitates in the fractures and pores of monazite, but U was removed from monazite by the hydrothermal fluid, which agrees with [12]. Monazite from the hydrothermal quartz veins was texturally and chemically different from the Ce-monazite of the unaltered granite. It had systematically lower Ca, U, Th, and Y, and higher Si, P, and LREE than the monazite from the unaltered granite (Table 3), because it was dissolved and had a hydrothermal origin. The analytical totals of monazite decreased from the unaltered granite to the altered granite and mineralized quartz veins (Table 3), but the losses in U, Th, and Y contents in the same direction were progressively much higher.

Xenotime from the unaltered granite was characterized by higher U contents than the xenotime from the altered granite, and both had higher U contents than the xenotime from the hydrothermal veins (Table 2). In the altered granite, xenotime crystals were zoned, with cores richer in U than their respective rims (Table 2, Figure 4d), indicating a loss of U in the crystal rims. So, the hydrothermal alteration of granite caused a loss of U in xenotime, which was higher in the crystal rims.

Due to their similar ionic radii, rare earth elements (REE), particularly the heavy rare earth elements (HREE), substituted for Y in the xenotime structure [55,56]. The xenotime from the mineralized quartz veins was richer in Y and HREE than the xenotime from the unaltered and altered granite (Table 2). In all of the xenotime crystals, the LREE contents were very low, because they were not readily incorporated into the xenotime structure. Besides HREE, xenotime may accommodate significant concentrations of Th and U [16]. Uranium was always enriched relative to Th in the analyzed xenotime, and the highest Th content (mean of 0.014 a.p.f.u.) was found in the xenotime from the mineralized quartz veins, which had the lowest U contents (Table 2). There was no significant difference between the Th, Y, and HREE contents of the xenotime from the unaltered and altered granites; so, the difference found in the U contents was due to alteration, indicating the mobilization of U from the xenotime structure. This is also supported by the impoverishment of the rims of crystals in U relative to their cores (Table S3).

According to [49], the dominant complex coupled substitution in xenotime, involving both crystallographic sites in the lattice, is thorite (ThSiO_4). Figure 3i shows the intergrowth between xenotime and thorite. Compositional exchange between the two end-members, thorite and xenotime, was continuous because the minerals were isostructural [16], but the xenotime analyzed had very low contents of Th (Table 2).

Although xenotime and monazite have different structures, they have some compositional and structural similarities [56]. Figure 3i also shows the intergrowth between xenotime and monazite,

which have equal numbers of structural PO_4 tetrahedra and REO_9 polyhedra; however, monazite incorporates larger, light rare earth elements (LREE) in the REO_9 polyhedron [57].

In the altered granite and the mineralized quartz veins, the altered zircon was enriched in uranium. According to [13], uraninite is occasionally associated with zircon as minute inclusions or also as thin exsolutions, whose grain size does not allow accurate analysis. The uraninite included in zircon will promote its faster metamitization and alteration. Metamict zircon under hydrothermal conditions loses Si, U, Th, and Pb [58,59]. There was a significant loss of Si, but also a strong enrichment in U, in the altered zircon (Table 2). The BSE image did not show concentrations of U in the restricted areas within zircon grains, but it did show a continuous increase of U contents toward the altered rims and fractures of zircon crystals (Figure 3a in [15]). The oxidizing conditions of the hydrothermal fluid did not allow the precipitation of uraninite.

Zircon from the altered granite was richer in P, Fe, Y, U, La + Ce, and Pb, and poorer in Si, Zr, and Hf; it also had lower analytical totals than the zircon from the unaltered granite. So, the hydrothermally alteration of zircon was expressed by a decrease in the analytical totals of Si, Zr, and Hf, and an increase in the analytical totals of Fe, Y, La + Ce, Pb, U, and P. In altered granite, the core of zircon crystals had a chemical composition similar to zircon from the unaltered granite with very low or no uranium contents. However, the crystal rims had up to 0.62 wt. % UO_2 , and the crystal rims from the mineralized quartz veins had up to 15.07 wt. % UO_2 (Table S3), but reached 18 wt. % UO_2 [16]. The authors [60] also found a gain in U in the rims of hydrothermally altered zircon grains. The altered zircon and zircon rims also had high contents of P_2O_5 (Table S3). An enrichment in P was accompanied by an enrichment in Y (Table 3) and HREE, promoting the formation of solid solutions with xenotime [61]. The structural relationship between xenotime and zircon is reflected by their occurrence as intimate intergrowths in the related quartz veins [15]. However, it should be noted that a few crystals show a depletion in U in their rims, as found by [58,59] in the rims of altered zircon grains. The U-enrichment in the rims of the hydrothermally altered zircon grains in the quartz veins was associated with the presence of Fe oxyhydroxides, which promoted the formation of new small U-phosphates at the margins of the altered zircon from U-rich supergenetic solutions. Zircon in the altered granite, especially in the crystal rims, was also rich in Fe (up to 0.66 wt. % Fe_2O_3 , Table S3). So, the enrichment in U was a compositional feature that was characteristic of hydrothermally altered zircon, and associated with high Fe contents [15].

Apatite from the altered granite and mineralized quartz veins was fractured, and showed dissolution (Figure 3e). It was replaced by thorite, xenotime, and monazite, which filled the fractures. Apatite from the altered granite was poorer in P, Ca, U, and F, and richer in Si, Th, Y, La, and Ce than the apatite from the unaltered granite (Table 3). So, the hydrothermal alteration of apatite led to a loss of P, Ca, U, and F in the hydrothermal fluid, while the enrichment in Si, Th, Y, La, and Ce led to the formation of hydrothermal thorite, xenotime, and monazite from apatite [62–68]. Furthermore, the most fractured and altered crystals had very low analytical totals, and showed a significant loss in P (Table 3). In general, the apatite from the mineralized quartz veins was the richest in U and F (means of 0.13 wt. % UO_2 and 2.76 wt. % F, Table 3). Some apatite crystals that were associated with or replaced by uranium phosphates had the highest uranium contents (1.09 wt. % UO_2 , Table 4), and were richer in Fe; however, their P contents were lower than those from the apatite that was not associated with the U-phosphates.

Figures 3j and 4e show (meta)saleeite crystals growing at the surface of apatite, indicating the precipitation of (meta)saleeite at the reaction interfaces of dissolving apatite under local saturation. According to [22], the observation that saleeite occurred where apatite has been replaced indicates that the local geochemical conditions in contact with apatite crystals are sufficient to precipitate saleeite at the expense of P by local saturation. Apatite is rare in quartz veins, which is probably due to its completely replacement by saleeite. The formation of the saleeite and meta-saleeite in the mineralized quartz veins is directly related to weathered apatite and Fe oxyhydroxides. Uranium was released during uraninite, coffinite, thorite, monazite, and xenotime dissolutions, and the phosphorus was

released essentially from apatite dissolution. The magnesium was released from chlorite alteration to clay minerals and Fe oxyhydroxides.

Chlorite from the altered granite was characterized by the average chemical formula $(\text{Mg}_{2.99}\text{Fe}_{5.87}\text{Mn}_{0.07}\text{Al}_{2.81})_{\Sigma 12.44}[(\text{Si}_{5.50}\text{Al}_{2.50})_{\Sigma 8.00}\text{O}_{20}](\text{OH})_{16}$, ($n = 19$), and is classified as clinochlore. Uranium was not detected in this chlorite from the altered granite, which had a Mg/(Mg + Fe) ratio of 0.34. In the hydrothermal quartz veins, chlorite was clinochlore [62]. Chlorite occurred dispersed between quartz crystals and had an average formula $(\text{Mg}_{4.76}\text{Fe}_{4.20}\text{Mn}_{0.05}\text{Al}_{2.82})_{\Sigma 11.83}[(\text{Si}_{5.34}\text{Al}_{2.66})_{\Sigma 8.00}\text{O}_{20}](\text{OH})_{16}$, ($n = 26$), a Mg/(Mg + Fe) ratio of 0.53, and contained 0.04 wt. % UO_2 , but the clinochlore in contact with the U-phosphates from these veins had a composition $(\text{Mg}_{6.93}\text{Fe}_{2.42}\text{Mn}_{0.01}\text{Al}_{2.46}\text{U}_{0.01})_{\Sigma 11.83}[(\text{Si}_{5.62}\text{Al}_{2.38})_{\Sigma 8.00}\text{O}_{20}](\text{OH})_{16}$ ($n = 6$), a Mg/(Mg + Fe) ratio of 0.74, and on average 0.12 wt. % UO_2 [15].

The rims of chlorite crystals were richer in U than the respective cores, and they were related to Fe oxyhydroxides with high contents of UO_2 (up to 5.63 wt. %), P_2O_5 (up to 7.07 wt. %), and MgO (up to 2.5 wt. %) [15]. The anatase was not found in the unaltered and altered granites, but it occurred in the hydrothermal quartz veins, was rich in U, and its vacuoles and rims were replaced by U-bearing Fe oxyhydroxides. Thus, the altered rims of chlorite and anatase from mineralized quartz veins were replaced by U-bearing Fe oxyhydroxides, containing up to 5.6 wt. % UO_2 and 3.7 wt. % P_2O_5), which may have been due to nano-inclusions of U-phosphates.

7. Conclusions

The unaltered peraluminous Variscan Beiras granite contains uraninite and other uranium-bearing minerals such as thorite, xenotime, Ce-monazite, and zircon; its apatite also has some U.

Uraninite is rare in the hydrothermally altered granite, but it contains coffinite, which resulted from the hydrothermal alteration of uraninite. Uraninite, coffinite, thorite, xenotime, Ce-monazite, zircon, apatite, chlorite and anatase, from either the altered granite and/or hydrothermal mineralized quartz veins, were dissolved and vacuolated. The rims of uraninite, coffinite, thorite, xenotime and Ce-monazite were poorer in U than their respective cores, indicating uranium removal to the meteoric fluid, while the altered rims of zircon, apatite, chlorite and anatase crystals were richer in U than their respective cores. The enrichment in U was related to the presence of Fe minerals, Fe oxyhydroxides, and altered apatite, as Fe and P have a high capacity to adsorb U.

The U-mineralization in the quartz veins occurred in the intersection of two fault systems, and the paragenetic sequence had three phases. The first phase produced silicates, sulfides and phosphates (apatite, xenotime, monazite), while the precipitation of the U-phosphates occurred in the third supergenic phase. The large and deep Variscan faults along which the granite had been hydrothermally altered were reactivated by Alpine tectonism. Subsequently, this gave rise to a deep circulation of meteoric waters within the granite and along the quartz veins, which were heated and became enriched in uranium by solubilization, and the complete remobilization of U-bearing minerals locally. These fluids were responsible for the growth of a new mineral assemblage in the hydrothermal quartz veins, where the dissolved U was fixed on the altered surface of minerals such as zircon and apatite and chlorite by adsorption, or by the precipitation as uranium minerals such as saleeite and meta-saleeite.

This precipitation at the surface of the new Fe-minerals was the main factor responsible for U retention within the quartz veins, leading to the uranium phosphate mineralization of Vale de Abrutiga.

The uranium released from uraninite (and thorite?) in the hydrothermal alteration of the granite was immobilized in coffinite. Later, the meteoric hot fluids promoted a high dissolution of (the remaining) uraninite, coffinite, thorite, xenotime, and monazite in the granite, and became enriched in uranium.

Close to the surface, where the oxygen content was high, the brecciated quartz veins acted as structural traps where Fe was immobilized as Fe oxyhydroxides. The precipitation of U-phosphates occurred on the surface of these Fe oxyhydroxides and on the weathered surface of apatite,

immobilizing the uranium. The Fe oxyhydroxides may also have adsorbed some U, P, and Mg, and their transformation to hematite or goethite lead to the precipitation of U-phosphate minerals.

Supplementary Materials: The following are available online at www.mdpi.com/2076-3263/8/3/95/s1.

Acknowledgments: Thanks are due to B.J. Wood for the EUGF—Bristol Facility contract ERBFMGECT 980128 for the use of the electron-microprobe at the University of Bristol, UK; M.R. Machado Leite and J.M. Farinha Ramos for the use of the electron-microprobe at the Geological and Mining Institute, S. Mamede de Infesta, Portugal; National Uranium Enterprise Administration for having provided the rock samples. This research was carried out in the programme of Geosciences Centre, University of Coimbra, Portugal, by the Foundation for Science and the Technology (SFRH/BPD/71030/2010) and by the Geobiotec Centre (UI/D/GEO/04035/2013). Thanks are due to Nova Science Publishers, which gave the permission to use the material published in a chapter “Uranium minerals from a Portuguese Variscan peraluminous granite, its alteration, and related uranium-quartz veins”, ISBN-978-1-60692-573-7. The manuscript benefited from careful and constructive reviews by three anonymous reviewers.

Author Contributions: Marina M. S. Cabral Pinto and Fernanda Guimarães conceived and designed the experiments; Marina M. S. Cabral Pinto and Fernanda Guimarães performed the experiments; Marina M. S. Cabral Pinto, Fernanda Guimarães and Paulo B. Silva analyzed the data; Ana M. R. Neiva and Maria M. V. G. Silva contributed reagents/materials/analysis tools; Marina M. S. Cabral Pinto wrote the paper.

Conflicts of Interest: The authors declare no conflict of interest.

References

1. Fleischer, M.; Mandarino, J.A. *Glossary of Mineral Species*; Mineralogical Record: Tucson, AZ, USA, 1995.
2. Boekhout, F.; Gérard, M.; Kanzari, A.; Michel, A.; Déjeant, A.; Galois, L.; Calas, G.; Descostes, M. Uranium migration and retention during weathering of a granitic waste rock pile. *Appl. Geochem.* **2015**, *58*, 123–135. [[CrossRef](#)]
3. Burns, P.C.; Finch, R.J. *Uranium: Mineralogy, Geochemistry and the Environment*; Mineralogical Society of America: Chantilly, VA, USA, 1999; Volume 38, p. 679.
4. Finch, R.; Murakami, T. Systematics, Paragenesis of U minerals. In *Uranium: Mineralogy, Geochemistry and the Environment*; Mineralogical Society of America: Chantilly, VA, USA, 1999; Volume 38, pp. 91–180.
5. Coteló Neiva, J.M. Jazigos portugueses de minérios de urânio e sua gênese. In *Engineering Geology and Geological Resources*; Coteló Neiva, J., Ferreira, M.R.P.V., Eds.; Coimbra University Press: Coimbra, Portugal, 2003; Volume 1, pp. 15–76.
6. Neiva, A.M.R.; Carvalho, P.C.S.; Antunes, I.M.H.R.; Santos, A.C.T.; Cabral Pinto, M.M.S. Spatial and temporal variability of surface water and groundwater before and after the remediation of a Portuguese uranium mine area. *Chem. Erde-Geochem.* **2015**, *75*, 345–356. [[CrossRef](#)]
7. Kanzari, A.; Gerard, M.; Boekhout, F.; Galois, L.; Calas, G.; Descostes, M. Impact of incipient weathering on uranium migration in granitic waste rock piles from former U mines (Limousin, France). *J. Geochem. Explor.* **2017**, *183*, 114–126. [[CrossRef](#)]
8. Cuney, M.; Friederich, M. Physicochemical and crystal-chemical controls on accessory mineral paragenesis in granitoids: Implications for uranium metallogenesis. *Bull. Minerl.* **1987**, *110*, 235–247.
9. Cabral Pinto, M.M.C.; Silva, M.M.V.G.; Ferreira da Silva, E.A.; Dinis, P.A.; Rocha, F. Transfer processes of potentially toxic elements (PTE) from rocks to soils and the origin of PTE in soils: A case study on the island of Santiago (Cape Verde). *J. Geochem. Explor.* **2017**. [[CrossRef](#)]
10. Plant, J.A.; Simpson, P.R.; Smith, B.; Windley, B.F. Uranium ore deposits-products of the radioactive earth. In *Uranium: Mineralogy, Geochemistry and the Environment*; Burns, P.C., Finch, R., Eds.; Mineralogical Society of America: Chantilly, VA, USA, 1999; Volume 38, pp. 255–319.
11. Förster, H.-J. The chemical composition of uraninite in Variscan granites of the Erzgebirge, Germany. *Mineral. Mag.* **1999**, *63*, 239–252. [[CrossRef](#)]
12. Hecht, L.; Cuney, M. Hydrothermal alteration of monazite in the Precambrian crystalline basement of the Athabasca Basin (Saskatchewan, Canada): Implications for the formation of unconformity-related uranium deposits. *Mineral. Depos.* **2000**, *35*, 791–795. [[CrossRef](#)]
13. Förster, H.-J. Composition and origin of intermediate solid solutions in the system thorite–xenotime–zircon–coffinite. *Lithos* **2006**, *88*, 35–55. [[CrossRef](#)]

14. Gaines, R.V.; Skinner, H.C.W.; Foord, E.E.; Mason, B.; Rosenzweig, G.A.; King, V.T.; Dowty, E. *Dana's New Mineralogy*, 8th ed.; Wiley and Sons: New York, NY, USA, 1997; p. 1819.
15. Cabral Pinto, M.M.S.; Silva, M.M.V.G.; Neiva, A.M.R. Geochemistry of U-bearing minerals from the Vale de Abrutiga uranium mine area, Central Portugal. *J. Mineral. Geochem.* **2008**, *185*, 183–198. [[CrossRef](#)]
16. Hetherington, C.J.; Harlov, D.E. Metasomatic thorite and uraninite inclusions in xenotime and monazite from granitic pegmatites, Hidra anorthosite massif, southwestern Norway: Mechanics and fluid chemistry. *Am. Mineral.* **2008**, *93*, 806–820. [[CrossRef](#)]
17. Abdelouas, A.; Lutze, W.; Nuttall, H.E. Uranium contamination in the subsurface; characterization and remediation. *Rev. Mineral. Geochem.* **1999**, *38*, 433–473.
18. Kotzer, T.G.; Kyser, T.K. U and Pb isotopic and chemical variations in uraninite: Implications for determining the temporal and fluid history of ancient terranes. *Am. Mineral.* **1993**, *78*, 1262–1274.
19. Murphy, W.M.; Shock, E.L. Environmental aqueous geochemistry of actinides. *Rev. Mineral.* **1999**, *38*, 221–253.
20. Neiva, A.M.R.; Carvalho, P.C.S.; Antunes, I.M.H.R.; Cabral Pinto, M.M.S.C.; Santos, A.C.T.; Cunha, P.P.; Costa, M.M. Spatial variability of soils and stream sediments and the remediation effects in a Portuguese uranium mine area. *Chem. Erde-Geochem.* **2016**, *76*, 501–518. [[CrossRef](#)]
21. Hsi, C.-K.D.; Langmuir, D. Adsorption of uranyl onto ferric oxyhydroxides: Application of the surface complexation site-binding model. *Geochim. Cosmochim. Acta* **1985**, *49*, 1931–1941.
22. Murakami, T.; Ohnuhi, T.; Isobe, H. Mobility of uranium during weathering. *Am. Mineral.* **1997**, *82*, 888–899. [[CrossRef](#)]
23. Lottermoser, B.G.; Asheley, T.P.M. Tailings dam seepage at the rehabilitated Mary Kathleen uranium mine, Australia. *J. Geochem. Explor.* **2005**, *85*, 19–137. [[CrossRef](#)]
24. Matos Dias, J.M. Perspectivas geoconómicas dos jazigos uraníferos portugueses. *Geonovas* **1982**, *1*, 33–39.
25. Cabral Pinto, M.M.S.; Silva, M.M.V.G. The Vale de Abrutiga uranium phosphates mine, central Portugal. *Chem. Erde-Geochem.* **2007**, *67*, 251–252. [[CrossRef](#)]
26. Pagel, M. Acteurs de Distribution et Concentration de L'uranium et du Thorium Dans Quelques Granites de la Chaîne Hercynienne d'Europe. Ph.D. Thesis, L'Institut National Polytechnique de Lorraine, Vandœuvre-lès-Nancy, France, 1981; p. 566.
27. Pinto, M.M.S.C.; Silva, M.M.V.G.; Neiva, A.M.R. Pollution of Water and Stream Sediments associated with the Vale de Abrutiga Uranium mine, Central Portugal. *J. Mine Water Environ.* **2004**, *23*, 66–75. [[CrossRef](#)]
28. Silva, M.M.V.G.; Neiva, A.M.R. Geochemistry of Hercynian peraluminous granites and their minerals from Carregal do Sal-Nelas-Lagares da Beira area, Central Portugal. *Chem. Erde-Geochem.* **2000**, *59*, 329–349.
29. Silva, M.M.V.G.; Neiva, A.M.R.; Whitehouse, M.J. Geochemistry of enclaves and host granites from the Nelas area, central Portugal. *Lithos* **2000**, *50*, 153–170. [[CrossRef](#)]
30. Poty, B.; Leroy, J.; Cathelineau, M.; Cuney, M.; Friedrich, M.; Lespinasse, M.; Turpin, L. Uranium deposits spatially related to granites in the French part of the Hercynian orogen. In *Vein Type Uranium Deposits*; IAEA-TC-361; International Atomic Energy Agency: Vienna, Austria, 1986; pp. 215–246.
31. Smith, D.K., Jr. Uranium mineralogy. In *Uranium Geochemistry, Mineralogy, Geology, Exploration and Resources*; De Vivo, B., Ippolito, F., Capaldi, G., Simpson, P.R., Eds.; Institute of Mining and Metallurgy: London, UK, 1984; pp. 43–88.
32. Langmuir, D. Uranium solution-mineral equilibria at low temperatures with applications to sedimentary ore deposits. *Geochim. Cosmochim. Acta* **1978**, *42*, 547–569. [[CrossRef](#)]
33. Parks, G.A.; Pohl, D.C. Hydrothermal solubility of uraninite. *Geochim. Cosmochim. Acta* **1988**, *52*, 863–875. [[CrossRef](#)]
34. Finch, R.J.; Ewing, R.C. The corrosion of uraninite under oxidizing conditions. *J. Nucl. Mater.* **1992**, *190*, 133–156. [[CrossRef](#)]
35. Janeczek, J.; Ewing, R.C. Structural formula of uraninite. *J. Nucl. Mater.* **1992**, *190*, 128–132. [[CrossRef](#)]
36. Percy, E.C.; Prikryl, J.D.; Murphy, W.M.; Leslie, B.W. Alteration of uraninite from the Nopal I deposit, Peña Blanca District, Chihuahua, Mexico, compared to degradation of spent nuclear fuel in the proposed U.S. high-level nuclear waste repository at Yucca Mountain, Nevada. *Appl. Geochem.* **1994**, *9*, 713–732. [[CrossRef](#)]
37. Fayek, M.; Janeczek, J.; Ewing, R.C. Mineral chemistry and oxygen isotopic analyses of uraninite, pitchblende and uranium alteration minerals from the Cigar Lake deposit, Saskatchewan, Canada. *Appl. Geochem.* **1997**, *12*, 549–565. [[CrossRef](#)]

38. Jensen, K.A.; Ewing, R.C.; Gauthier-Lafaye, F. Uraninite: A 2 Ga spent nuclear fuel from the natural fission reactor at Bangombe´ in Gabon, West Africa. *Mater. Res. Soc. Symp. Proc.* **1997**, *465*, 1209–1218. [[CrossRef](#)]
39. Jerden, J.R.; Sinha, A.K. Phosphate based immobilization of uranium in an oxidizing bedrock aquifer. *Appl. Geochem.* **2003**, *18*, 823–843. [[CrossRef](#)]
40. Evins, L.Z.; Jensen, A.K.; Ewing, R.C. Uraninite recrystallization and Pb loss in the Oklo and Bangombe natural fission reactors, Gabon. *Geochim. Cosmochim. Acta* **2005**, *69*, 1589–1606. [[CrossRef](#)]
41. Bruno, J.; Ewing, R.C. Spent nuclear fuel. *Elements* **2006**, *2*, 343–349. [[CrossRef](#)]
42. Deditius, A.P.; Utsunomiya, A.; Ewing, R.C. Fate of trace elements during alteration of uraninite in a hydrothermal vein-type U-deposit from Marshall Pass, Colorado, USA. *Geochim. Cosmochim. Acta* **2007**, *71*, 4954–4973. [[CrossRef](#)]
43. Alexandre, P.; Kyser, T.K. Effects of cationic substitutions and alteration in uraninite, and implications for the dating of uranium deposits. *Can. Mineral.* **2005**, *43*, 1005–1017. [[CrossRef](#)]
44. Speer, J.A. The actinide orthosilicates. *Rev. Mineral.* **1982**, *5*, 113–135.
45. Lumpkin, G.R.; Chakoumakos, B.C. Chemistry and radiation effects of thorite-group minerals from the Harding pegmatite, Taos County, New Mexico. *Am. Mineral.* **1988**, *73*, 1405–1419.
46. Smits, G. (U,Th)-bearing silicates in reefs of the Witwatersrand, South Africa. *Can. Mineral.* **1989**, *27*, 643–655.
47. Janeczek, J.; Ewing, R.C. X-ray powder diffraction study of annealed uraninite. *J. Nucl. Mater.* **1991**, *185*, 66–77. [[CrossRef](#)]
48. Rubin, J.N.; Henry, C.H.; Price, J.G. Hydrothermal zircons and zircon overgrowths, Sierra Blanca Peaks, Texas. *Am. Mineral.* **1989**, *74*, 865–869.
49. Harlov, D.E.; Aandersson, U.B.; Förster, H.-J.; Nyström, J.O.; Dulski, P.; Broman, C. Apatite–monazite relations in the Kiirunavaara magnetite–apatite ore, northern Sweden *Chem. Geol.* **2002**, *191*, 47–72.
50. Harlov, D.E.; Wirth, R.; Förster, H.-J. An experimental study of dissolution–reprecipitation in fluorapatite: Fluid infiltration and the formation of monazite. *Contrib. Mineral. Petrol.* **2005**, *150*, 268–286. [[CrossRef](#)]
51. Finger, F.; Broska, I.; Roberts, M.P.; Schermaier, A. Replacement of primary monazite by apatite–allanite–epidote coronas in an amphibolite facies granite gneiss from the eastern Alps. *Am. Mineral.* **1998**, *83*, 248–258. [[CrossRef](#)]
52. Thomson, B.M.; Smith, C.L.; Busch, R.D.; Siegel, M.D. Removal of metals and radionuclides using apatite and other natural sorbents. *J. Environ. Eng.* **2003**, *129*, 492–499. [[CrossRef](#)]
53. Wark, D.A.; Miller, C.F. Accessory mineral behavior during differentiation of a granite suite: Monazite, xenotime and zircon in the Sweetwater Wash pluton, southeastern California, U.S.A. *Chem. Geol.* **1993**, *110*, 49–67. [[CrossRef](#)]
54. Ni, Y.; Hughes, J.M. Crystal chemistry of the monazite and xenotime structures. *Am. Mineral.* **1995**, *80*, 21–26. [[CrossRef](#)]
55. Broska, I.; Williams, C.T.; Geza Nagy, M.J. Alteration and breakdown of xenotime-(Y) and monazite-(Ce) in granitic rocks of the Western Carpathians, Slovakia. *Lithos* **2005**, *82*, 71–83. [[CrossRef](#)]
56. Geisler, T.; Pidgeon, R.T.; Van Bronswijk, W.; Kurtz, R. Transport of uranium, thorium, and lead in metamict zircon under low-temperature hydrothermal conditions. *Chem. Geol.* **2002**, *191*, 141–154. [[CrossRef](#)]
57. Geisler, T.; Pidgeon, R.T.; Kurtz, R.; Van Bronswijk, W.; Schleicher, H. Experimental hydrothermal alteration of partially metamict zircon. *Amer. Mineral.* **2003**, *88*, 1496–1513. [[CrossRef](#)]
58. Horie, K.; Hidakab, H.; Gauthier-Lafaye, F. Elemental distribution in apatite, titanite and zircon during hydrothermal alteration: Durability of immobilization mineral phases for actinides. *Phys. Chem. Earth* **2008**, *33*, 962–968. [[CrossRef](#)]
59. Deer, W.A.; Howie, R.A.; Zussman, J. *Rock-Forming Minerals—Orthosilicates*, 2nd ed.; The Geological Society: London, UK, 1997; Volume 1, p. 919.
60. Bailey, S.W. Summary of recommendations of AIPEA nomenclature committee. *Clay Miner.* **1980**, *15*, 85–93. [[CrossRef](#)]
61. Janeczek, J.; Ewing, R.C. Dissolution and alteration of uraninite under reducing conditions. *J. Nucl. Mater.* **1992**, *190*, 157–173. [[CrossRef](#)]
62. Ordoñez-Regis, E.; Romero Guzmán, E.T.; Ordoñez Regil, E.N. Surface modification in natural fluorapatite after uranyl solution treatment. *J. Radioanal. Nucl. Chem.* **1999**, *240*, 541–554. [[CrossRef](#)]
63. Arey, J.S.; Seaman, J.; Bertch, P.M. Immobilization of Uranium in Contaminated Sediments by Hydroxyapatite Addition. *Environ. Sci. Technol.* **1999**, *33*, 337–342. [[CrossRef](#)] [[PubMed](#)]

64. Townsend, K.J.; Miller, C.F.; D'Andrea, J.L.; Ayers, J.C.; Harrison, T.M.; Coath, C.D. Low temperature replacement of monazite in the Ireteba granite, Southern Nevada: Geochronological implications. *Chem. Geol.* **2000**, *172*, 95–112. [[CrossRef](#)]
65. Jeanjean, J.; Rouchaud, J.C.; Tran, L.; Fedoroff, M. Sorption of uranium and other heavy metals on hydroxyapatite. *J. Radioanal. Nucl. Chem.* **2005**, *201*, 529–539. [[CrossRef](#)]
66. Conca, J.L.; Wright, J. An Apatite II permeable reactive barrier to remediate groundwater containing Zn, Pb and Cd. *Appl. Geochem.* **2006**, *21*, 1288–1300. [[CrossRef](#)]
67. Simon, F.G.; Biermann, V.; Peplinski, B. Uranium removal from groundwater using hydroxyapatite. *Appl. Geochem.* **2008**, *23*, 2137–2145. [[CrossRef](#)]
68. Wellman, D.M.; Glovack, J.N.; Parker, K.; Richards, E.L.; Pierce, E.M. Sequestration and retention of uranium(VI) in the presence of hydroxylapatite under dynamic geochemical conditions. *Environ. Chem.* **2008**, *5*, 40–50. [[CrossRef](#)]



© 2018 by the authors. Licensee MDPI, Basel, Switzerland. This article is an open access article distributed under the terms and conditions of the Creative Commons Attribution (CC BY) license (<http://creativecommons.org/licenses/by/4.0/>).